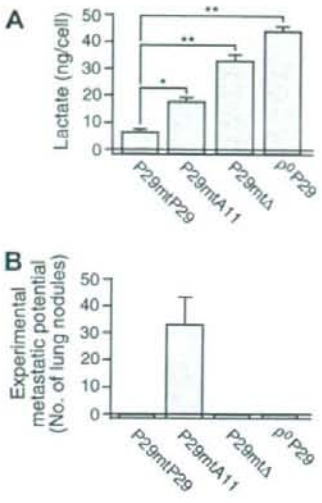

Fig. 3. Effects of the enhanced lactate production on expression of metastatic potential. (A) The lactate level in culture medium. The P29mtP29 cybrids and ρ^0P29 cells were used as cells with normal mitochondrial respiratory function and without mitochondrial respiratory function, respectively. Bars represent the means ± S.D. ($n = 3$). *, $P < 0.05$; **, $P < 0.005$. (B) Experimental metastatic potential. We counted number of nodules formed in the lung after inoculation of the cybrids into the tail vein. Enhanced glycolysis is not necessarily correlated with expression of high metastatic potential. Bars represent the means ± S.D. ($n = 6$).

while P29mtP29 cybrids expressing normal respiratory function did not form lung nodules (Fig. 3B). These observations suggest that the mtDNA mutations that induce ROS overproduction can be responsible for metastasis, but the mtDNA mutation or mtDNA depletion that induces the Warburg effect alone are not responsible for metastasis at least in Lewis lung carcinoma cell lines.

4. Discussion

Our recent report demonstrated that complex I defects caused by the mtDNA mutations and resultant ROS overproduction reversibly control metastasis, and that ROS overproduction controls metastasis not by induction of genetic instability or by upregulation of glycolysis, but by upregulation of metastasis-related nuclear genes [16]. However, since complex I defects simultaneously induce up-regulation of glycolysis in addition to ROS overproduction, it is still possible that upregulation of glycolysis caused by complex I defects alone can be responsible for metastasis. We examined this possibility by isolation of the P29mtΔ cybrids that expressed enhanced glycolysis, but did not express ROS overproduction (Fig. 2), and showed that metastasis was not induced in the P29mtΔ cybrids (Fig. 3). Since enhanced glycolysis under normoxia, i.e., the Warburg effect, caused by mitochondrial respiration defects alone did not induce metastasis in the P29mtΔ cybrids, the induction of high metastatic potential in the P29mtA11 cybrids [16] would be due to ROS overproduction, but not to the Warburg effect caused by complex I defects.

The remaining question is whether enhanced glycolysis may induce oncogenic transformation of normal cells to develop tumors, even though it did not induce malignant progression of tumor cells to develop metastasis (Fig. 3B). This possibility would be excluded, since mito-mice expressing enhanced glycolysis due to accumulation ΔmtDNA4696 [23,24] did not show any bias to form tumors in their tissues (Ishikawa et al., unpublished observations). Thus, enhanced glycolysis induced by mitochondrial respiration defects would not be involved in both tumor and metastasis development at least in tissues of mito-mice and in mouse tumor cells used in this study. To provide direct evidence of whether the Warburg effect induced by mitochondrial respiration defects is not involved in tumor development, we are going to isolate embryonic fibroblast cell lines possessing ΔmtDNA4696 from the mito-mice, and examine whether they are prone to develop tumors.

Acknowledgments: This work was supported by Grants-in-Aid for Scientific Research (S) from the Japan Society for Promotion of Science (JSPS), by Grants-in-Aid for Creative Scientific Research from JSPS, and by Grants-in-Aid for Scientific Research on Priority Areas from The Ministry of Education, Culture, Sports, Science and Technology of Japan (MEXT) to J.-I.H. This work was also supported by grants for a Research Fellowship from JSPS for Young Scientists to K.I. and by Grants-in-Aid for Third Term Comprehensive Control Research for Cancer from the Ministry of Health, Labour, and Welfare and for Scientific Research from MEXT to K.T.

References

[1] Allen, J.A. and Coombs, M.M. (1980) Covalent binding of polycyclic aromatic compounds to mitochondrial and nuclear DNA. Nature 287, 244–245.
[2] Backer, J.M. and Weinstein, I.B. (1980) Mitochondrial DNA is a major cellular target for a dihydrodiol-epoxide derivative of benzo(a)pyrene. Science 209, 297–299.
[3] Shay, J.W. and Werbin, H. (1987) Are mitochondrial DNA mutations involved in the carcinogenic process? Mutat. Res. 186, 149–160.
[4] Polyak, K., Li, Y., Zhu, H., Lengauer, C., Willson, J.K.V., Markowitz, S.D., Trush, M.A., Kinzler, K.W. and Vogelstein, B. (1998) Somatic mutations of the mitochondrial genome in human colorectal tumors. Nat. Genet. 20, 291–293.
[5] Fliss, M.S., Usadel, H., Caballero, O.L., Wu, L., Buta, M.R., Eleff, S.M., Jen, J. and Sidransky, D. (2000) Facile detection of mitochondrial DNA mutations in tumors and bodily fluids. Science 287, 2017–2019.
[6] Penta, J.S., Johnson, F.M., Wachsman, J.T. and Copeland, W.C. (2001) Mitochondrial DNA in human malignancy. Mutat. Res. 488, 119–133.
[7] Taylor, R.W. and Turnbull, D.M. (2005) Mitochondrial DNA mutations in human disease. Nat. Rev. Genet. 6, 389–402.
[8] Czarnecka, A.M., Golik, P. and Bartnik, E. (2006) Mitochondrial DNA mutations in human neoplasia. J. Appl. Genet. 47, 67–78.
[9] Gallardo, M.E., Moreno-Loshuertos, R., López, C., Casqueiro, M., Silva, J., Bonilla, F., Rodríguez de Córdoba, S. and Enríquez, J.A. (2006) m.6267G>A: A recurrent mutation in the human mitochondrial DNA that reduces cytochrome *c* oxidase activity and is associated with tumors. Hum. Mutat 27, 575–582.
[10] Hayashi, J.-I., Yonekawa, H. and Tagashira, Y. (1989) Nuclear but not mitochondrial genome involvement in 3-methylcholanthrene-induced expression of tumorigenicity in mouse somatic cells. Cancer Res. 49, 4715–4720.
[11] Akimoto, M., Niikura, M., Ichikawa, M., Yonekawa, H., Nakada, K., Honma, Y. and Hayashi, J.-I. (2005) Nuclear DNA but not mtDNA controls tumor phenotypes in mouse cells. Biochem. Biophys. Res. Commun. 327, 1028–1035.
[12] Hayashi, J.-I., Werbin, H. and Shay, J.W. (1986) Effects of normal human fibroblast mitochondrial DNA on segregation of

HeLaTG mitochondrial DNA and on tumorigenicity of HeLaTG cells. Cancer Res. 46, 4001–4006.
[13] Hayashi, J.-I., Takemitsu, M. and Nonaka, I. (1992) Recovery of the missing tumorigenicity in mitochondrial DNA-less HeLa cells by introduction of mitochondrial DNA from normal cells. Somat. Cell Mol. Genet. 18, 123–129.
[14] Kaneda, H., Hayashi, J.-I., Takahama, S., Taya, C., Fischer Lindahl, K. and Yonekawa, H. (1995) Elimination of paternal mitochondrial DNA in intraspecific crosses during early mouse embryogenesis. Proc. Natl. Acad. Sci. USA 92, 4542–4546.
[15] Shitara, H., Hayashi, J.-I., Takahama, S., Kaneda, H. and Yonekawa, H. (1998) Maternal inheritance of mouse mtDNA in interspecific hybrids: segregation of the leaked paternal mtDNA followed by the prevention of subsequent paternal leakage. Genetics 148, 851–857.
[16] Ishikawa, K., Takenaga, K., Akimoto, M., Koshikawa, N., Yamaguchi, A., Imanishi, H., Nakada, K., Honma, Y. and Hayashi, J.-I. (2008) ROS-generating mitochondrial DNA mutations can regulate tumor cell metastasis. Science 320, 661–664.
[17] Baysal, B.E., Ferrell, R.E., Willett-Brozick, J.E., Lawrence, E.C., Myssiorek, D., Bosch, A., van der Mey, A., Taschner, P.E., Rubinstein, W.S., Myers, E.N., Richard 3rd, C.W., Cornelisse, C.J., Devilee, P. and Devlin, B. (2000) Mutations in SDHD, a mitochondrial complex II gene, in hereditary paraganglioma. Science 287, 848–851.
[18] Niemann, S. and Muller, U. (2000) Mutations in SDHC cause autosomal dominant paraganglioma, type3. Nat. Genet. 26, 268–270.
[19] Gottlieb, E. and Tomlinson, I.P. (2005) Mitochondrial tumor suppressors: a genetic and biochemical update. Nat. Rev. Cancer 5, 857–866.
[20] Christofk, H.R., Vander Heiden, M.G., Harris, M.H., Ramanathan, A., Gerszten, R.E., Wei, R., Fleming, M.D., Schreiber, S.L. and Cantley, L.C. (2008) The M2 splice isoform of pyruvate kinase is important for cancer metabolism and tumour growth. Nature 452, 230–233.
[21] Inoue, K., Ito, S., Takai, D., Soejima, A., Shisa, H., LePecq, J.-B., Segal-Bendirdjian, E., Kagawa, Y. and Hayashi, J.-I. (1997) Isolation of mitochondrial DNA-less mouse cell lines and their application for trapping mouse synaptosomal mitochondrial DNA with deletion mutations. J. Biol. Chem. 272, 15510–15515.
[22] Miyabayashi, S., Haginoya, K., Hanamizu, H., Iinuma, K., Narisawa, K. and Tada, K. (1989) Defective pattern of mitochondrial respiratory enzymes in mitochondrial myopathy. J. Inherit Metab. Dis. 12, 373–377.
[23] Inoue, K., Nakada, K., Ogura, A., Isobe, K., Goto, Y., Nonaka, I. and Hayashi, J.-I. (2000) Generation of mice with mitochondrial dysfunction by introducing mouse mtDNA carrying a deletion into zygotes. Nat. Genet. 26, 176–181.
[24] Nakada, K., Inoue, K., Ono, T., Isobe, K., Ogura, A., Goto, Y.-i., Nonaka, I. and Hayashi, J.-I. (2001) Inter-mitochondrial complementation: mitochondria-specific system preventing mice from expression of disease phenotypes by mutant mtDNA. Nat. Med. 7, 934–940.

MOLECULAR AND CELLULAR BIOLOGY, Jan. 2008, p. 293–301
0270-7306/08/$08.00+0 doi:10.1128/MCB.00473-07

Vol. 28, No. 1

Altered Quality Control in the Endoplasmic Reticulum Causes Cortical Dysplasia in Knock-In Mice Expressing a Mutant BiP▽

Naoya Mimura,[1,2] Shigeki Yuasa,[3] Miho Soma,[3] Hisayo Jin,[1] Keita Kimura,[2] Shigemasa Goto,[2] Haruhiko Koseki,[4] and Tomohiko Aoe[1]*

Department of Anesthesiology[1] and Department of Medicine and Clinical Oncology,[2] Chiba University Graduate School of Medicine, 1-8-1 Inohana, Chuo-ku, Chiba City, Chiba 260-8670, Department of Ultrastructural Research, National Institute of Neuroscience, National Center of Neurology and Psychiatry, 4-1-1 Ogawahigashi, Kodaira, Tokyo 187-8502,[3] and Laboratory for Developmental Genetics, RIKEN Research Center for Allergy and Immunology, 1-7-22 Suehiro, Tsurumi, Yokohama 230-0045,[4] Japan

Received 20 March 2007/Returned for modification 21 June 2007/Accepted 2 October 2007

Binding immunoglobulin protein (BiP) is an endoplasmic reticulum (ER) molecular chaperone that is central to ER function. We examined knock-in mice expressing a mutant BiP in order to elucidate physiological processes that are sensitive to BiP functions during development and adulthood. The mutant BiP lacked the retrieval sequence that normally functions to return BiP to the ER from the secretory pathway. This allowed us to examine the effects of a defect in ER function without completely eliminating BiP function. The homozygous mutant BiP neonates died after birth due to respiratory failure. Besides that, the mutant BiP mice displayed disordered layer formation in the cerebral cortex and cerebellum, a neurological phenotype of *reeler* mutant-like malformation. Consistent with the phenotype, Cajal-Retzius (CR) cells did not secrete reelin, and the expression of reelin was markedly reduced posttranscriptionally. Furthermore, the reduction in the size of the whole brain and the apparent scattering of CR cells throughout the cortex, which were distinct from the *reeler* phenotype, were also seen. These findings suggest that the maturation and secretion of reelin in CR cells and other factors related to neural migration may be sensitive to aberrant ER quality control, which may cause various neurological disorders.

Proteins destined for the secretory pathway are inserted into the endoplasmic reticulum (ER) cotranslationally and subjected to quality control (12, 25). Aberrant protein folding due to extracellular stimuli such as ischemia, hypoxia, and genetic mutations results in the accumulation of misfolded proteins in the ER, which causes ER stress and initiates the unfolded protein response (UPR) (35, 39) that enhances the capacity for ER quality control by reducing general protein synthesis (18), producing ER chaperones, and promoting ER-associated degradation (4, 6). A failure of this adaptation mechanism may cause cellular dysfunction and cell death, resulting in diverse human disorders (24, 26) such as neurodegenerative disease (21, 23), cardiomyopathy (15), and diabetes (17, 34). Furthermore, mutant mouse models have revealed that the UPR plays a vital role during normal development by increasing protein synthesis, as necessary, of dedicated secretory cells (46) such as pancreatic beta cells (38), plasma cells (37), hepatocytes (36), and alveolar type II epithelial cells (29). Inadequate adaptation to these physiological demands may lead to diverse diseases.

ER molecular chaperones and folding enzymes such as binding immunoglobulin protein (BiP), calnexin, and protein disulfide isomerase facilitate the correct folding or degradation of these newly synthesized proteins as well as of misfolded proteins. BiP, also called the 78-kDa glucose-regulated protein (GRP78), is a member of the heat shock protein 70 (HSP70) family of proteins and is one of the most abundant ER chaperones, assisting in protein translocation, folding, and degradation (31). ER chaperones localize to the ER by two mechanisms: retention and retrieval (40). BiP is retained in the ER by interacting with other ER proteins and the ER matrix. When misfolded proteins accumulate in the ER, BiP is secreted from the ER together with the misfolded proteins, where it assists with protein refolding, or it helps in the degradation of these proteins (16, 47). In post-ER compartments, the carboxyl-terminal Lys-Asp-Glu-Leu (KDEL) sequence of BiP is then recognized by the KDEL receptor, which facilitates the return of BiP to the ER (27, 30).

The complete depletion of BiP has lethal effects on mammalian early embryonic cells (28). *Saccharomyces cerevisiae* BiP (Kar2p) is essential for survival, while the deletion of the retrieval sequence (His-Asp-Glu-Leu [HDEL] in yeast) is dispensable because the UPR is activated, and the loss of the chaperone in the ER is compensated for (3). Therefore, to elucidate physiological processes that are sensitive to BiP functions during development and adulthood in multicellular organisms, we produced knock-in mice expressing a mutant BiP in which the retrieval sequence was deleted by homologous recombination. The mutant BiP mice died within several hours after birth due to impaired pulmonary surfactant biosynthesis and respiratory failure (29). We also found disordered layer formation in the cerebral cortex and cerebellum in the mutant BiP neonates. Although altered quality control in the ER due to mutant BiP may affect the expression of several proteins with regard to corticogenesis, we found that the expression of one such protein, reelin, secreted by Cajal-Retzius (CR) cells (9), was markedly reduced. These findings suggest that committed secretory cells, such as CR cells, have a threshold of

* Corresponding author. Mailing address: Department of Anesthesiology, Chiba University Graduate School of Medicine, 1-8-1 Inohana, Chuo-ku, Chiba City, Chiba 260-8670, Japan. Phone: 81-43-226-2573. Fax: 81-43-226-2156. E-mail: taoe@faculty.chiba-u.jp.

▽ Published ahead of print on 22 October 2007.

protein-folding capacity to cope with the normal physiological protein overload in the ER during development, and BiP plays an important role.

MATERIALS AND METHODS

Reagents. The following antibodies were used: mouse monoclonal antibody (mAb) CR50 against reelin (a gift from M. Ogawa, Brain Science Institute, RIKEN, Japan), rabbit antiserum against the hemagglutinin (HA) epitope (Zymed, San Francisco, CA), mouse mAb G10 against reelin, rabbit antiserum against Dab1 (Chemicon, Temecula, CA), rabbit antiserum against Dab1 (phospho-Y220) (Abcam, Cambridge, United Kingdom), mouse mAb EP5 against fibronectin, mouse mAb 6A6 against very-low-density lipoprotein receptor (VLDLR), rabbit antiserum against CHOP/GADD153, rabbit antiserum against ubiquitin, goat polyclonal antiserum against BiP/GRP78, mouse mAb J-3 against Cdk5 (Santa Cruz Biotechnology, Santa Cruz, CA), mouse mAb 9E10 against the Myc epitope (ATCC, Manassas, VA), mouse mAb against γ-tubulin (Sigma Chemical, St. Louis, MO), mouse mAb SPA-827 against BiP (KDEL sequence) (Stressgen, Ann Arbor, MI), Cy2-conjugated donkey antibody against rabbit immunoglobulin G (IgG), and Cy3-conjugated donkey antibody against mouse IgG (Jackson Immunoresearch Laboratories, West Grove, PA). TO-PRO-3 and a Slow-Fade antifade kit were purchased from Molecular Probes (Invitrogen, Carlsbad, CA).

Plasmids and transfection. A *reelin* cDNA (pCrl) was kindly provided by T. Curran (St. Jude Children's Research Hospital, Memphis, TN) (10). To express a Myc-tagged mutant BiP lacking the KDEL sequence, a cDNA encoding a mutant BiP with residues 1 to 650 was obtained by PCR using rat *BiP* cDNA (a gift from H. R. B. Pelham, MRC Laboratory of Molecular Biology, United Kingdom). The PCR product was subcloned into a pcDNA3.1 Myc-His vector (Invitrogen, Carlsbad, CA). Transfection was performed with the calcium phosphate method (20).

Mutant BiP mice. We used homologous recombination to establish knock-in mice expressing BiP lacking the carboxyl-terminal KDEL sequence (29). The missing KDEL sequence was replaced by an HA tag. All animal experimental procedures were performed in accordance with a protocol approved by the Institutional Animal Care Committee of Chiba University, Chiba, Japan.

Western blot. The brains removed from the mice and cells were homogenized in a buffer containing 0.4% Nonidet P-40, 0.2% *N*-lauroylsarcosine, 30 mM Tris-HCl (pH 8.0), 1 mM EDTA, 10 μg ml^{-1} aprotinin, 10 μg ml^{-1} leupeptin, and 30 μg ml^{-1} *N*-acetyl-L-leucinal-L-lecinal-L-norleucinal (ALLN; Sigma Chemical). The lysates were boiled in sodium dodecyl sulfate-polyacrylamide gel electrophoresis sample buffer and separated by sodium dodecyl sulfate-polyacrylamide gel electrophoresis under reducing conditions. Gels were transferred onto polyvinylidene fluoride membranes (Immobilon-P; Millipore Corp., Billerica, MA), blocked with 5% nonfat dry milk in the buffer described above, incubated with a primary antibody followed by peroxidase-conjugated donkey anti-goat, anti-mouse, or anti-rabbit IgG, and developed by chemiluminescence (ECL; Amersham Pharmacia Biotech, Buckinghamshire, United Kingdom). Imaging was obtained by using LAS1000 and Image Gauge software (Fuji Photo Film Co. Ltd., Tokyo, Japan).

Primary neuronal culture. Cortical neurons of mouse embryos were derived from embryos at day 17.5 to 18.5 according to standard procedures (1). After removing the meninges, cortical lobes were isolated in phosphate-buffered saline (PBS), dissected into small pieces, and digested with 0.25% trypsin and 0.02% DNase I in PBS with 5% glucose at 37°C for 20 min. Trypsin was then neutralized with a half volume of horse serum, and the solution was centrifuged at 440 × *g* for 5 min at 4°C. The resultant cells were triturated in Dulbecco's modified Eagle's medium (DMEM)-F-12 medium containing 10% fetal bovine serum using a siliconized Pasteur pipette and scattered at about 2×10^5 to 4×10^5 cells/cm^2 on plates coated with poly-L-lysine (Sigma). Cells were maintained in DMEM–F-12 medium containing 10% fetal bovine serum–1% penicillin-streptomycin for 3 days at 37°C and then replaced with opti-MEM (Invitrogen) containing 1% of an insulin-transferrin-selenium A mixture (ITS; Invitrogen) and antibiotics. On the following day, the supernatants were collected, centrifuged using a table-top machine at 440 × *g* for 5 min at 4°C, and concentrated by centrifugation (YM50; Millipore). The neurons were treated with control or reelin-containing medium (prepared as previously described) (8) at 37°C for 20 min and collected for Western blotting. 293T cells were transfected with full-length mouse reelin expression construct pCrl. The following day, the cells were washed with serum-free DMEM and maintained in opti-MEM containing 1% ITS and antibiotics. After three more days, the conditioned medium was collected, centrifuged at 440 × *g* for 5 min at 4°C, and used as the reelin-containing medium.

Confocal and immunofluorescence microscopy of primary neurons. Cells on coverslips were fixed in cold methanol for 10 min at −20°C and then processed as previously described (20). The stained cells were examined by either confocal laser scanning microscopy (LSM510 fitted with krypton and argon lasers; Carl Zeiss, Oberkochen, Germany) or fluorescence microscopy (Axiovert 200 M; Carl Zeiss).

Northern blot. Northern blot analysis was done as previously described (15). The expression level of the *reelin* and *BiP* mRNAs was assessed relative to that of β-*actin* mRNA using densitometry by Image Gauge software (Fuji Photo Film).

In situ hybridization histochemistry. *reelin* cDNA extending from nucleotides 4716 to 5476 (GenBank accession number U24703) (9) was cloned into the pGEM-T Easy vector (Promega, Madison, WI). In vitro transcription from *reelin* cDNA was performed using a digoxigenin-UTP RNA labeling kit (Roche Applied Science, Mannheim, Germany) to prepare the antisense and sense cRNA probes according to the manufacturer's instructions.

The brains of mouse embryos at embryonic day 15.5 (E15.5) were fixed with 4% paraformaldehyde dissolved in 0.1 M sodium phosphate buffer (pH 7.4), and postfixed overnight at 4°C with the same fixative. The brains were embedded in 2% agar in PBS and sliced coronally into 150-μm sections with a Microslicer (DTK-3000; Dosaka EM, Kyoto, Japan). Hybridization and detection procedures were performed as described below. The free-floating sections were incubated with proteinase K (20 μg/ml) in 0.1% Tween 20 in PBS (PBST) for 10 min at room temperature. Sections were rinsed with PBST, refixed in 4% paraformaldehyde for 20 min, and again rinsed with PBST three times each for 20 min. Sections were prehybridized in hybridization buffer (50% formamide, 5× SSC [1× SSC is 0.15 M NaCl plus 0.015 M sodium citrate], 50 μg/ml heparin, 0.1% Tween 20, 5 mg/ml torula RNA) for 30 min at 65°C. Subsequently, sections were hybridized overnight at 65°C with digoxigenin-UTP-labeled antisense or sense riboprobes (0.2 μg/ml) in the hybridization buffer. Sections were then sequentially rinsed in 2× SSCT (0.1% Tween 20 in SSC)–50% formamide twice each for 30 min at 65°C, 2× SSCT for 15 min at 65°C, and 0.2× SSCT twice each for 30 min at 65°C and then incubated overnight with alkaline phosphatase-coupled anti-digoxigenin antibody (1:4,000 dilution; Roche Applied Science, Mannheim, Germany). After washing with PBST three times and then once with 0.1 M Tris-HCl (pH 8.2), sections were stained by use of a solution prepared from FastRed tablets (Roche Applied Science, Mannheim, Germany) according to the manufacturer's instruction and then washed with PBST three times. Sections were then coverslipped with 80% glycerol, and fluorescence images were obtained directly with a confocal laser scanning microscope (LSM5 Pa; Zeiss, Oberkochen, Germany). No labeling was detectable in the control sections that were hybridized with the sense riboprobe (data not shown).

Immunohistochemistry. Pregnant mice were deeply anesthetized by Nembutal, and embryos were removed by cesarean section. The embryos were fixed by transcardiac perfusion with 4% paraformaldehyde in PBS, and the heads were further immersion fixed for 12 h at 4°C. Embryonic brains were then embedded in 3% agar in PBS, and sections at a thickness of 200 μm were prepared on a Microslicer (Dosaka EM, Kyoto, Japan). The sections were incubated with 10% normal goat serum in PBS for 30 min to block nonspecific antibody binding and then incubated with a mixture of CR50 mouse monoclonal antibody (1:200 dilution) (32) and rabbit anti-calretinin (1:2,000; Swant, Switzerland) in PBS for 12 h at 4°C. The sections were rinsed with PBS and then incubated with a mixture of Cy2-conjugated anti-rabbit IgG (1:100; Jackson Immunoresearch) and Cy3-conjugated anti-mouse IgG (1:200; Chemicon) in PBS for 2 h at 4°C. For calbindin immunohistochemistry of the cerebellum, rabbit anti-calbindin (1:2,000; Swant) was used as the primary antibody, and Cy2-conjugated anti-rabbit IgG was the secondary antibody. The sections were then rinsed with PBS and mounted onto glass slides with 80% glycerol. For counterstaining with a DNA dye, the sections immunostained with anti-calbindin antibody were stained with TO-PRO-3 (Invitrogen) and mounted with SlowFade (Molecular Probes). The sections were observed under a confocal laser scanning microscope (LSM5 Pa; Carl Zeiss).

BrdU labeling. Bromodeoxyuridine (BrdU) (80 mg · kg^{-1}) was administered intraperitoneally to pregnant mice at the E13 or E15 three times a day (at 10:00, 16:00, and 22:00). At E18, the embryos were removed by cesarean section and perfusion fixed as mentioned above. The brains were embedded in agar, and sections with a thickness of 200 μm were prepared and incubated with 2 N HCl for 1 h at room temperature. The sections were then rinsed with PBS, treated with 10% normal goat serum, and then incubated with a mouse mAb against BrdU (1:50; Becton Dickinson, San Jose, CA) for 12 h. After rinsing with PBS, the sections were incubated with Alexa 488-conjugated goat anti-mouse IgG

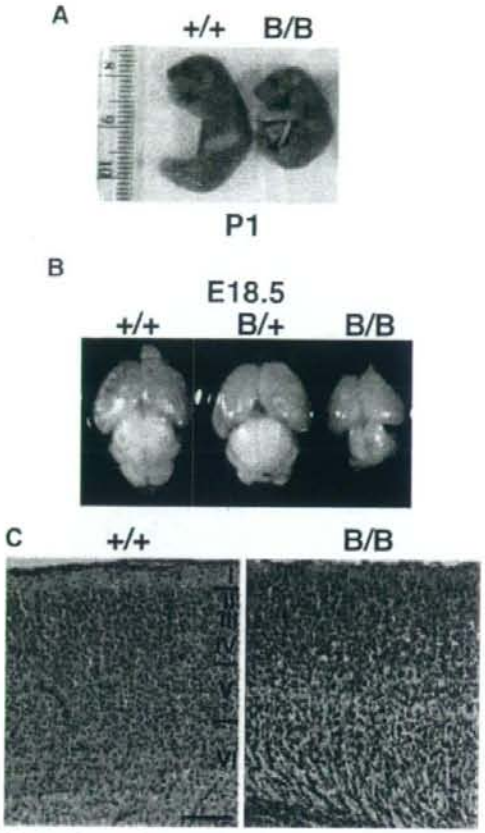

FIG. 1. Absence of the KDEL retrieval sequence from BiP impairs brain development. (A) Newborns at P1. (B) Brains from E18.5 embryos. (C) At E18, large numbers of neurons are distributed in the superficial layer of the mutant (right), in contrast to the cell-sparse layer I of the control (left). (C) Hematoxylin-eosin staining. Scale bar, 100 μm. B/B, homozygous; B/+, heterozygous; +/+, wild type.

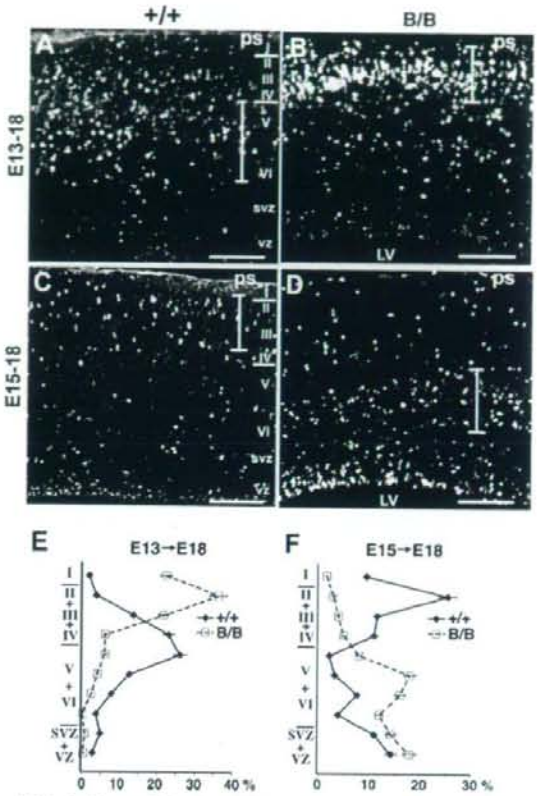

FIG. 2. Mutant BiP mice exhibit an outside-in pattern of neocortical layer formation. Shown is birth date analysis of the neocortical neurons. (A, B, and E) BrdU was administered at E13, and the distribution of the labeled cells was examined at E18. In control mice, heavily labeled cells were stratified in the lower layers (layers V and VI) (A), in contrast to the significant reduction of labeled cells in the lower layers and their significant increase in the superficial layer in the mutant (B). A quantitative analysis is represented in E. (C, D, and F) BrdU was administered at E15, and the distribution of the labeled cells was examined at E18. In the control, heavily labeled cells reached the upper layers (layers II and III), and the still-migrating cells were also found in the lower layer (C). In contrast, only small numbers of the labeled cells reached the upper layers (layers II and III), and a large proportion of them were distributed in the lower layer in the mutant (D). A quantitative analysis is represented in F. The graphs in E and F represent the averages ± standard errors of the means of BrdU-labeled cells in each layer of four serial sections from a representative brain of each genotype. The extent of the layers in that the cortical neurons were intensely labeled with BrdU is indicated by a vertical bar in each picture. B/B, homozygous mutant; +/+, wild-type mice; LV, lateral ventricle; ps, pial surface; svz, subventricular zone; vz, ventricular zone; I to VI, neocortical layers. Scale bars, 100 μm.

(1:500 dilution; Invitrogen) in PBS for 2 h at 4°C. The sections were then rinsed again with PBS and mounted onto glass slides with glycerol. Immunolocalization was observed under a confocal laser scanning microscope. The primordium of the somatosensory cortex was divided into 10 layers from the ventricular surface to the pial surface. The densities of BrdU-labeled cells in each layer were determined in four serial sections from a representative brain of each genotype. BrdU-labeled cells in the defined area of each section of the neocortical primordium were counted from the ventricular surface to the pial surface to obtain the total numbers of labeled cells, and the average percentages of the labeled cells in each layer were plotted on a histogram.

RESULTS

Defective neocortical layer formation in mutant BiP mice. The homozygous mutant BiP mice were born at the expected Mendelian ratio, and they died within 1 day after birth due to respiratory failure (29). They moved and responded to painful stimuli but appeared pale and were significantly smaller than wild-type mice (Fig. 1A). Among the various organs, the mutant brain, including the cerebral cortex and cerebellum, was substantially smaller than those of wild-type mice (Fig. 1B), suggesting that the brain was particularly affected by the BiP mutation. In fact, the neocortical stratification at E18, as observed with hematoxylin-eosin staining, was defective in the mutant BiP mice. The mutant brain had a relatively high density of neurons in neocortical layer I (Fig. 1C, right), in contrast

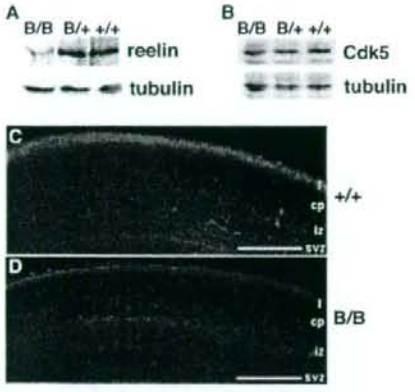

FIG. 3. Significant downregulation of reelin expression in superficial layer I of the mutant BiP neocortical primordium. (A and B) The levels of expression of reelin, Cdk5, and γ-tubulin in brains of E18.5 embryos were evaluated by Western blotting. (C and D) At E16, intense reelin immunoreactivity was found in the superficial layer of the control (C), but immunoreactivity was significantly reduced in the mutant brain (D). Scale bars, 200 μm. cp, cortical plate; iz, intermediate zone; svz, subventricular zone; I, layer I; B/B, homozygous mice; B/+, heterozygous mutant mice; +/+, wild-type mice.

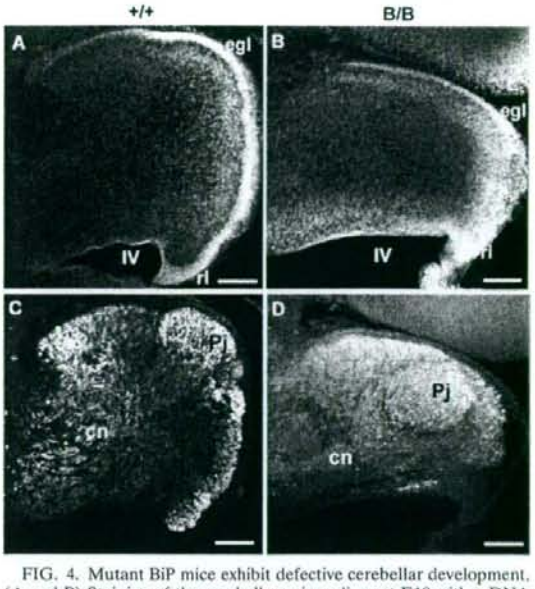

FIG. 4. Mutant BiP mice exhibit defective cerebellar development. (A and B) Staining of the cerebellar primordium at E18 with a DNA dye, TO-PRO-3. The cerebellum of the homozygote (B) is much smaller than that of the wild type (A). An EGL is formed in both genotypes, but the progression of EGL formation in the caudorostral direction is retarded in the homozygote (B). (C and D) Purkinje cell distribution in the cerebellum at E18. Calbindin-immunoreactive Purkinje cells are distributed in the cortical layer in the cerebellum of the control (C). In contrast, large numbers of immunoreactive cells stay in the subcortical region of the mutant cerebellum (D). Scale bars, 100 μm. B/B, homozygous mice; +/+, wild-type mice; cn, cerebellar nucleus; egl, EGL; Pj, Purkinje cell layer; rl, rhombic lip; IV, the fourth ventricle.

to a low density of neuronal arrangement in the control (Fig. 1C, left).

Cortical neurogenesis occurs in the ventricular zone, and the new neurons migrate through other new neurons to the marginal zone and then move to their final destination during embryogenesis. To further investigate the defect in layer formation during neocortical development, birth date analysis of the neocortical neurons was carried out by BrdU labeling (Fig. 2A to D). Neuronal precursors in the ventricular zone became labeled with BrdU during proliferation and migrated after the final mitosis through earlier-born neurons to the cortical plate in normal corticogenesis. When BrdU was administered at E13, heavily labeled cells were distributed in forming layers V and VI, and lightly labeled cells that repeated mitosis after BrdU incorporation were distributed in the upper layers at E18 in the control (Fig. 2A and E), as reported previously by Caviness (7). In the mutant, however, heavily labeled cells were distributed in the upper layer up to superficial layer I, and few labeled cells were observed in the lower layer at E18 (Fig. 2B and E). When BrdU was administered at E15, in the control, the heavily labeled cells reached upper layers II and III at E18 (Fig. 2C and F), as reported previously by Caviness (7), but in the mutant, only a small number of heavily labeled cells reached these upper layers, and most of the labeled cells were distributed in the lower layer (Fig. 2D and F). These findings indicate that, in the mutant brain, the earlier-born neurons reached the superficial layer and remained there and that the later-born neurons did not reach the upper layer, remaining in the lower layer. The mutant BiP mice exhibited an outside-in pattern of neocortical layer formation, in contrast to the inside-out pattern in the control (7), indicating that neocortical layer formation was impaired.

Mutant BiP mice have reduced expression of reelin. The above-described findings suggested that aberrant neocortical formation is due to the defects in layer formation, like a deficiency in reelin signaling in a *reeler* mutant malformation (9, 13) or a deficiency in Cdk5 signaling (33). Indeed, analysis of the embryonic cerebral neocortex revealed significantly reduced reelin expression by Western blotting and immunoreactivity in superficial layer I of the mutant BiP mice (Fig. 3A, C, and D), while the expression of Cdk5 was preserved (Fig. 3B). These results are consistent with the fact that reelin is a secretory protein that may interact with BiP in the ER, whereas Cdk5 is a cytosolic protein that is apart from BiP.

Because *reeler* malformation is also well documented in the cerebellum with regard to the migration defect of Purkinje cells (48), the structure of the cerebellum was examined at E18. The growth of the mutant cerebellum was significantly retarded as shown by staining with DNA dye (Fig. 4A and B). Although the external granular layer (EGL) was formed in both genotypes, the development of an EGL migrating tangentially from the rhombic lip was significantly retarded in the mutant BiP mice (Fig. 4A and B). A large number of Purkinje cells remained in the subcortical region, in contrast to the cortical arrangement of Purkinje cells in the control (Fig. 4C and D). Hippocampal layer formation showed little defect in the mutant BiP mice based on hematoxylin-eosin-stained sections (data not shown).

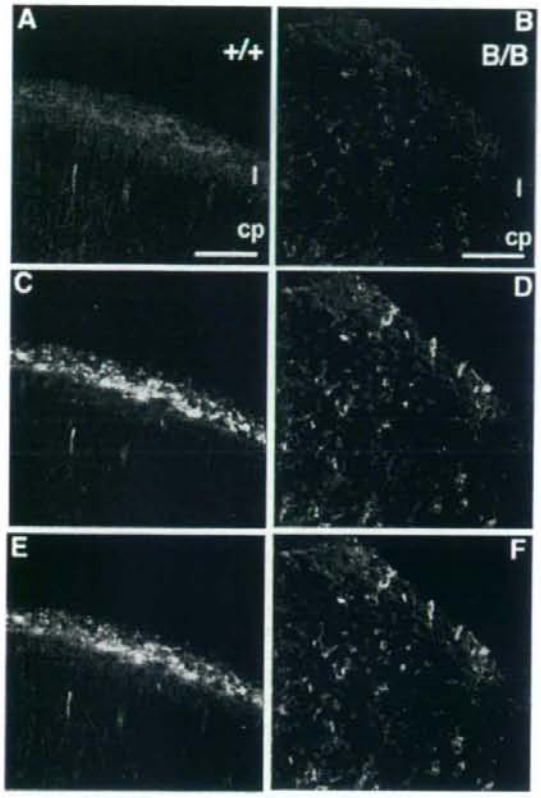

FIG. 5. Distribution of CR cells in the neocortical primordium. At E16, reelin immunoreactivity (red) in the superficial layer (I) of control (A) and mutant (B) brains was present. Calretinin-immunopositive CR cells (green) were found in the superficial layers of both control (C) and mutant (D) mice. Reelin immunoreactivity colocalizes with calretinin in CR cells in the control (E) (A and C were merged), but reelin immunoreactivity is hardly detectable in the calretinin-positive cells in superficial layer I of the mutant (F) (B and D were merged). Furthermore, the cells that were double labeled with reelin and calretinin were found in the layers below the superficial layer in the mutant (F), although such cells were not detected in the wild type (E). Scale bars, 50 μm.

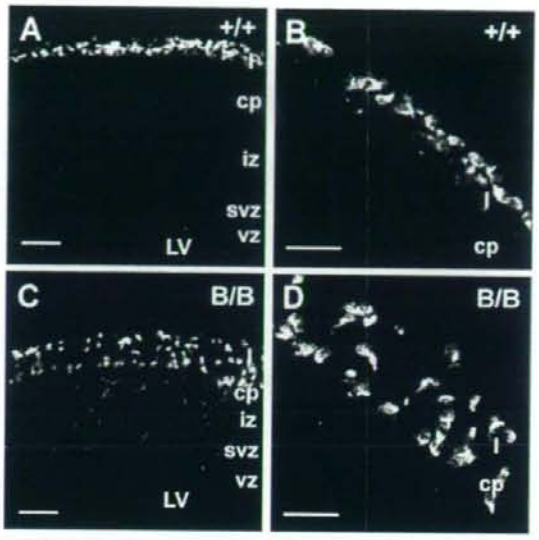

FIG. 6. The cells positive for *reelin* mRNA were scattered in the neocortical primordium of mutant BiP mice. The distribution of CR cells was further confirmed by in situ hybridization for *reelin* mRNA as the marker of CR cells in the neocortical primordium at E15.5. In the control, *reelin* mRNA-positive cells were situated in the superficial layer (layer I) as shown in A. The higher magnification of the upper cortical area represents the characteristic horizontal arrangement of CR cells (B). In contrast, *reelin* mRNA-positive cells were distributed from the superficial layer into the cortical plate in the homozygote (C). (D) Higher magnification of the upper cortical area in C. The random orientation of *reelin*-positive cells is evident. Scale bars, 100 μm in A and C and 50 μm in B and D.

The structure of the superficial layer of the neocortical primordium was further examined by double immunohistochemical labeling for both reelin and calretinin. Calretinin-immunopositive neurons, corresponding to CR cells in the neocortical primordium, were found in the superficial layer of the mutant BiP mice, but their numbers were significantly reduced, and reelin immunoreactivity was barely detected (Fig. 5B, D, and F), in contrast to the localization of reelin immunoreactivity in the calretinin-positive neurons in superficial layer I of the wild-type mice (Fig. 5A, C, and E). Some of calretinin-immunopositive CR cells of the mutant neocortex appeared in a disorganized, scattered pattern other than the marginal zone (Fig. 5F). This finding was confirmed by in situ hybridization histochemistry of the neocortical primordium by using *reelin* cRNA probe as the marker for CR cells. The cells positive for *reelin* mRNA formed a thin superficial layer in wild-type mice (Fig. 6A and B). In contrast, the cells positive for *reelin* mRNA were scattered in the upper layer of the neocortical primordium of the mutant BiP mice (Fig. 6C and D). These findings of in situ hybridization histochemistry correspond well with those of calretinin-immunoreactive cells. Furthermore, the present findings indicate that the transcription of the *reelin* gene takes place to a similar degree in both mutant and wild-type mice, but the reelin protein is significantly reduced in the CR cells of the mutant.

While this mouse does have features of a *reeler* mutant phenotype, such as an outside-in pattern of neocortical layer formation and the migration defect of Purkinje cells in the cerebellum, it also has other phenotypes in the brain that are distinct from the *reeler* phenotype. These include the reduction in the size of the whole brain and the apparent scattering of reelin- and calretinin-positive neurons throughout the cortex. This is not surprising since BiP likely has a multitude of substrates that are significant for brain development. Among them, we decided to focus on reelin since at least one of the reeler mutants has a defect in intracellular transport of reelin (11) rather than the production of reelin, and the transport mutant BiP may affect the folding and secretion of reelin.

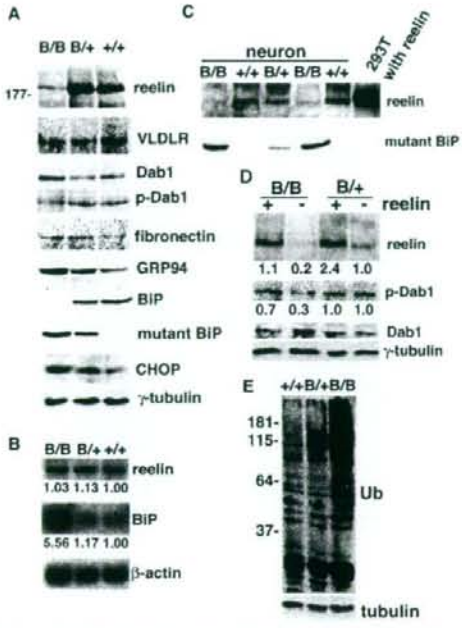

FIG. 7. Reelin expression is reduced posttranscriptionally in the mutant BiP brain. (A) The levels of expression of reelin, VLDLR, Dab1, tyrosine-phosphorylated Dab1 (p-Dab1), fibronectin, GRP94, BiP, mutant BiP, CHOP, and γ-tubulin in brains of E18.5 embryos were evaluated by Western blotting. In mutant BiP, the carboxyl-terminal KDEL sequence was replaced by an HA tag. (B) Northern blotting using probes for reelin, BiP, and β-actin mRNAs in brains at E18.5. The expression levels of reelin and BiP mRNAs were assessed by the relative ratio to β-actin mRNA. (C) Secretion of reelin and mutant BiP in the culture medium from the primary neurons and 293T cells transfected with reelin cDNA, as evaluated by Western blotting. (D) Primary neurons were treated with control (−) or reelin-containing medium (+) at 37°C for 20 min, collected, and subjected to Western blotting with antibodies against reelin, Dab1, tyrosine-phosphorylated Dab1, and γ-tubulin. The expression levels of reelin and tyrosine-phosphorylated Dab1 were assessed by the relative ratios to γ-tubulin. (E) Expression of ubiquitinated (Ub) proteins in the cerebrum at E18.5 embryos, as evaluated by Western blotting. B/B, homozygous mice; B/+, heterozygous mutant mice; +/+, wild-type mice.

Reelin secretion is impaired in the mutant BiP brain. Reelin is a large secreted glycoprotein (9) produced by some cortical neurons such as CR cells in the marginal zone during development. Reelin mediates cortical laminar formation through binding to VLDLR and apolipoprotein E receptor type 2 (ApoER2) on cortical neurons (8, 43). In *reeler* mice deficient in the reelin gene (9), the cortical neurons lack the ability to localize properly and settle inside the earlier-migrating neurons (7).

In E18.5 mice, we used an antibody directed against the amino terminus of reelin to detect a fragment of reelin (~180 kDa) in the wild-type cerebral cortex; however, these fragments were much less intense in the homozygous mutant BiP cortex (Fig. 7A), consistent with histological observations. Although VLDLR expression was equivalent between wild-type and mutant BiP cortices, dephosphorylated Dab1 accumulated in the mutant BiP brain, indicating that the reelin signaling pathway was inactivated there. The expression of another secreted glycoprotein, fibronectin, was preserved in the mutant brain. The reelin deficiency was not a consequence of reduced transcription, because *reelin* mRNA expression did not differ in control and mutant brains (Fig. 7B), consistent with the in situ hybridization experiment (Fig. 6). The expression of *BiP* mRNA as well as CHOP protein (a cell death-related transcriptional factor of the UPR) (50) was enhanced in the mutant brain (Fig. 7A and B), suggesting that the mutant brain suffered from ER stress.

Mutant BiP might impair the folding of reelin, leading to its degradation by the ER-associated degradation pathway or to its secretion as an immature form from the CR cells due to an escape from ER quality control. To test this possibility, we used primary neurons derived from embryonic brains and found a significant decrease in reelin secretion by the homozygous mutant BiP neurons compared with that of wild-type or heterozygous neurons (Fig. 7C). To investigate whether the homozygous mutant BiP neurons maintained their responsiveness to reelin stimulation, we incubated primary neurons with conditioned culture medium containing a severalfold physiological level of reelin secreted by 293T cells transiently transfected with reelin cDNA (Fig. 7D). Exogenous reelin seemed to be active on the homozygous neurons, leading to the activation of the reelin signaling pathway, as demonstrated by a reduced amount of Dab1 expression and an increased amount of phospho-Dab1 expression. On the other hand, the reelin signaling pathway in the heterozygous mutant cortical neurons seems to be constitutively active with endogenous reelin even without exogenous reelin stimulation. Thus, Dab1 expression and phosphorylation (Fig. 7D) are rather unchanged in the heterozygous mutant. These results suggest that the impaired secretion of reelin by the CR cells rather than defective responsiveness in the cortical neurons may be responsible for the neurological phenotype of *reeler* mutant-like malformations in mutant BiP mice. Thus, the impaired retrieval of BiP may promote the degradation of misfolded proteins by the ubiquitin/proteasome pathway. In fact, ubiquitinated proteins accumulated in the mutant cerebrum (Fig. 7E).

BiP may enhance the folding of reelin. Mutant BiP was detected in the ER (29), but a significant fraction was also secreted from cells because of the lack of the retrieval motif (KDEL) (Fig. 7C). We examined the subcellular localization of reelin to establish its relationship with mutant and wild-type BiP. Reelin colocalized with mutant BiP in the ER in primary neurons derived from heterozygous mutant BiP embryos; this was also the case in cortical neurons in the homozygous mutant postnatal brain, where the expression of reelin was reduced (Fig. 8A). To obtain further insight into the interaction of BiP and reelin, we performed cotransfection experiments in HeLa cells. Coexpression of reelin and wild-type BiP, but not the mutant BiP lacking the KDEL sequence, greatly enhanced the expression of reelin protein (reelin mRNA levels were equivalent in the two transfections) (Fig. 8B). These results suggest that BiP promotes the folding of reelin.

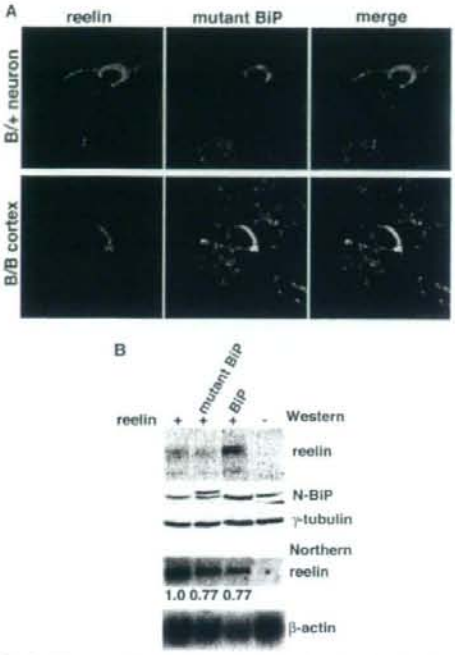

FIG. 8. BiP may enhance the maturation of reelin. (A) Subcellular localization of endogenous reelin and mutant BiP in primary neurons from the heterozygous (B/+) mutant BiP embryo and the cortex of the homozygous (B/B) mutant BiP embryo (E18.5), as evaluated by confocal laser scanning microscopy, with double labeling using a mouse mAb for reelin and a rabbit antiserum for HA. Scale bars, 10 μm. (B) HeLa cells were transiently transfected with reelin alone or cotransfected with either mutant BiP in which the KDEL sequence was replaced by a Myc tag or wild-type BiP (the Myc-tagged mutant BiP has a higher molecular weight than wild-type BiP). The levels of expression of reelin, BiP, and γ-tubulin were evaluated by Western blotting, and the levels of expression of *reelin* and β-*actin* mRNA were evaluated by Northern blotting. The expression level of *reelin* mRNA was assessed relative to that of β-*actin* mRNA.

DISCUSSION

We produced knock-in mice expressing a mutant BiP with the retrieval sequence deleted, which allowed us to examine the effects of a defect in the response to secretory pathway stress without completely eliminating BiP function, as would be the case with BiP knockout mice (28). The loss of BiP function was compensated for by the UPR in embryonic fibroblasts. However, neonates expressing mutant BiP suffered respiratory failure caused by the impaired secretion of pulmonary surfactant in alveolar type II epithelial cells (29). Furthermore, we observed abnormal corticogenesis in mutant BiP mice. Mutant BiP may predominantly affect dedicated secretory cells, such as alveolar type II cells and CR cells, in which active secretion is particularly important; thus, protein folding was probably affected in these cells. Indeed, we found an impaired secretion of reelin in CR cells, which may account for one aspect of cortical malformation in the cerebrum and cerebellum of mutant BiP mice. We also demonstrated increased Dab1 protein levels and a reduction in Dab1 tyrosine phosphorylation, which are consistent with a *reeler*-like phenotype. On the other hand, this mouse has other phenotypes in the brain that are distinct from the *reeler* phenotype. These include the reduction in the size of the whole brain and the apparent scattering of CR cells throughout the cortex, suggesting that mutant BiP may likely interfere with other substrates in addition to the reelin required for brain development.

The deletion of the retrieval sequence from BiP could have two possible effects. First, the lack of recycling of mutant BiP to the ER could impair the folding environment in the ER. This effect may be limited because constitutively active UPR compensates for it, and a sufficient amount of the functional mutant BiP, as long as it stays in the ER, may be produced for cell survival. Second, the impaired retrieval of mutant BiP may affect quality control in post-ER compartments. In addition to the ER itself, several studies have revealed that proper ER-to-Golgi apparatus transport and the subsequent retrieval/return of proteins and lipids to the ER may contribute to quality control (16, 19, 42, 45, 47). In this regard, the folding (and therefore function) of reelin may be dependent on the proper retrieval of BiP to the ER via interactions with the KDEL receptor.

Reelin is a large 3,461-residue secreted glycoprotein that has eight reelin repeats of ~350 residues each that contain an epidermal growth factor motif followed by a carboxyl-terminal 33 residues rich in basic amino acids (43). During embryogenesis, CR cells secrete reelin as homo-oligomers that function in cortical layer formation through binding to lipoprotein receptors on cortical neurons (44). Although the folding, intracellular transport, and oligomerization of reelin have not been characterized in detail, we found that reelin protein expression was impaired in mutant BiP mice, indicating that BiP may play a role in the maturation of reelin. Furthermore, we found that the expression levels of BiP mRNA and the CHOP protein were enhanced in the mutant brain, suggesting that the mutant brain might have suffered from ER stress. We speculate that the folding of the reelin protein may be vulnerable to impaired quality control in the ER and the post-ER compartments of mutant CR cells. If true, this assumption suggests that environmental stresses that perturb ER quality control may also impair the reelin signaling pathway and other factors, which may cause neuronal migration defects.

In addition to brain development, several studies suggested the possible role of reelin in the pathogenesis of human mental disorders such as schizophrenia, autism, bipolar disorder, and Alzheimer's disease (5, 14, 43). Because reelin signaling through ApoER2 in adult brains modulates synaptic plasticity and memory formation (2), the defective reelin signaling pathway may contribute to the pathogenesis of adult mental disorders. Reelin and ApoE share ApoER2 on cortical neurons (8), and ApoE inhibits reelin signaling by competing for binding to ApoER2. Interestingly, the E4 allele of ApoE increases the risk of developing sporadic forms of Alzheimer's disease.

In the meantime, the persistent accumulation of misfolded proteins beyond the capacity of ER quality control causes ER stress, leading to cellular dysfunction and cell death (24, 26). This process is thought to cause human mental disorders such as neurodegenerative diseases including Alzheimer's disease (23) and Parkinson's disease (21), bipolar disorders (22), and

ischemic neuronal injury (41). The involvement of impaired BiP function in neurodegenerative diseases has been reported in a mouse model where the disruption of SIL1, a cochaperone of BiP, caused protein accumulation and neurodegeneration (49). Thus, reelin signaling and ER quality control may be related to the pathogenesis of adult mental disorders, as seen in reeler mutant-like cerebral malformation in mutant BiP neonates.

The UPR is a ubiquitous mechanism in all cells to adapt to ER stress in pathological conditions, and BiP is an essential component of this system. Our results suggest that a physiological increase in the production of reelin and other factors in dedicated secretory cells like CR cells during neonatal periods may require the UPR and a proper folding capacity in the ER. Neuronal migration and stratification may be sensitive to environmental insults such as viral infection, hypoxia, and ischemia that perturb ER functions.

ACKNOWLEDGMENTS

We thank T. Nishino, K. Toshimori, and T. Yamashita for critical comments. We also thank M. Kashio for excellent technical assistance.

This work was supported by grants-in-aid for science research from the Ministry of Education, Culture, Sports, Science, and Technology of Japan to T.A. and grant 05-32 from NIBIO to S.Y.

REFERENCES

1. **Banker, G., and K. Goslin.** 1988. Developments in neuronal cell culture. Nature **336:**185–186.
2. **Beffert, U., E. J. Weeber, A. Durudas, S. Qiu, I. Masiulis, J. D. Sweatt, W. P. Li, G. Adelmann, M. Frotscher, R. E. Hammer, and J. Herz.** 2005. Modulation of synaptic plasticity and memory by Reelin involves differential splicing of the lipoprotein receptor Apoer2. Neuron **47:**567–579.
3. **Beh, C. T., and M. D. Rose.** 1995. Two redundant systems maintain levels of resident proteins within the yeast endoplasmic reticulum. Proc. Natl. Acad. Sci. USA **92:**9820–9823.
4. **Bonifacino, J. S., and A. M. Weissman.** 1998. Ubiquitin and the control of protein fate in the secretory and endocytic pathways. Annu. Rev. Cell Dev. Biol. **14:**19–57.
5. **Bothwell, M., and E. Giniger.** 2000. Alzheimer's disease: neurodevelopment converges with neurodegeneration. Cell **102:**271–273.
6. **Brodsky, J. L., and A. A. McCracken.** 1999. ER protein quality control and proteasome-mediated protein degradation. Semin. Cell Dev. Biol. **10:**507–513.
7. **Caviness, V. S., Jr.** 1982. Neocortical histogenesis in normal and reeler mice: a developmental study based upon [3H]thymidine autoradiography. Brain Res. **256:**293–302.
8. **D'Arcangelo, G., R. Homayouni, L. Keshvara, D. S. Rice, M. Sheldon, and T. Curran.** 1999. Reelin is a ligand for lipoprotein receptors. Neuron **24:**471–479.
9. **D'Arcangelo, G., G. G. Miao, S. C. Chen, H. D. Soares, J. I. Morgan, and T. Curran.** 1995. A protein related to extracellular matrix proteins deleted in the mouse mutant *reeler*. Nature **374:**719–723.
10. **D'Arcangelo, G., K. Nakajima, T. Miyata, M. Ogawa, K. Mikoshiba, and T. Curran.** 1997. Reelin is a secreted glycoprotein recognized by the CR-50 monoclonal antibody. J. Neurosci. **17:**23–31.
11. **de Bergeyck, V., K. Nakajima, C. Lambert de Rouvroit, B. Naerhuyzen, A. M. Goffinet, T. Miyata, M. Ogawa, and K. Mikoshiba.** 1997. A truncated Reelin protein is produced but not secreted in the 'Orleans' reeler mutation (Reln[rl-Orl]). Brain Res. Mol. Brain Res. **50:**85–90.
12. **Ellgaard, L., and A. Helenius.** 2003. Quality control in the endoplasmic reticulum. Nat. Rev. Mol. Cell Biol. **4:**181–191.
13. **Falconer, D. S.** 1951. Two new mutant, 'trembler' and 'reeler,' with neurological actions in the house mouse (Mus musculus L.). J. Genet. **50:**192–201.
14. **Fatemi, S. H.** 2005. Reelin glycoprotein: structure, biology and roles in health and disease. Mol. Psych. **10:**251–257.
15. **Hamada, H., M. Suzuki, S. Yuasa, N. Mimura, N. Shinozuka, Y. Takada, T. Nishino, H. Nakaya, H. Koseki, and T. Aoe.** 2004. Dilated cardiomyopathy caused by aberrant endoplasmic reticulum quality control in mutant KDEL receptor transgenic mice. Mol. Cell. Biol. **24:**8007–8017.
16. **Hammond, C., and A. Helenius.** 1994. Quality control in the secretory pathway: retention of a misfolded viral membrane glycoprotein involves cycling between the ER, intermediate compartment, and Golgi apparatus. J. Cell Biol. **126:**41–52.
17. **Harding, H. P., and D. Ron.** 2002. Endoplasmic reticulum stress and the development of diabetes: a review. Diabetes **51**(Suppl. 3):S455–S461.
18. **Harding, H. P., Y. Zhang, and D. Ron.** 1999. Protein translation and folding are coupled by an endoplasmic-reticulum-resident kinase. Nature **397:**271–274.
19. **Haynes, C. M., S. Caldwell, and A. A. Cooper.** 2002. An HRD/DER-independent ER quality control mechanism involves Rsp5p-dependent ubiquitination and ER-Golgi transport. J. Cell Biol. **158:**91–101.
20. **Hsu, V. W., N. Shah, and R. D. Klausner.** 1992. A brefeldin A-like phenotype is induced by the overexpression of a human ERD-2-like protein, ELP-1. Cell **69:**625–635.
21. **Imai, Y., M. Soda, H. Inoue, N. Hattori, Y. Mizuno, and R. Takahashi.** 2001. An unfolded putative transmembrane polypeptide, which can lead to endoplasmic reticulum stress, is a substrate of Parkin. Cell **105:**891–902.
22. **Kakiuchi, C., K. Iwamoto, M. Ishiwata, M. Bundo, T. Kasahara, I. Kusumi, T. Tsujita, Y. Okazaki, S. Nanko, H. Kunugi, T. Sasaki, and T. Kato.** 2003. Impaired feedback regulation of XBP1 as a genetic risk factor for bipolar disorder. Nat. Genet. **35:**171–175.
23. **Katayama, T., K. Imaizumi, N. Sato, K. Miyoshi, T. Kudo, J. Hitomi, T. Morihara, T. Yoneda, F. Gomi, Y. Mori, Y. Nakano, J. Takeda, T. Tsuda, Y. Itoyama, O. Murayama, A. Takashima, P. St. George-Hyslop, M. Takeda, and M. Tohyama.** 1999. Presenilin-1 mutations downregulate the signalling pathway of the unfolded-protein response. Nat. Cell Biol. **1:**479–485.
24. **Kaufman, R. J.** 2002. Orchestrating the unfolded protein response in health and disease. J. Clin. Investig. **110:**1389–1398.
25. **Kleizen, B., and I. Braakman.** 2004. Protein folding and quality control in the endoplasmic reticulum. Curr. Opin. Cell Biol. **16:**343–349.
26. **Kopito, R. R., and D. Ron.** 2000. Conformational disease. Nat. Cell Biol. **2:**E207–E209.
27. **Lewis, M. J., and H. R. Pelham.** 1990. A human homologue of the yeast HDEL receptor. Nature **348:**162–163.
28. **Luo, S., C. Mao, B. Lee, and A. S. Lee.** 2006. GRP78/BiP is required for cell proliferation and protecting the inner cell mass from apoptosis during early mouse embryonic development. Mol. Cell. Biol. **26:**5688–5697.
29. **Mimura, N., H. Hamada, M. Kashio, H. Jin, Y. Toyama, K. Kimura, M. Iida, S. Goto, H. Saisho, K. Toshimori, H. Koseki, and T. Aoe.** 2007. Aberrant quality control in the endoplasmic reticulum impairs the biosynthesis of pulmonary surfactant in mice expressing mutant BiP. Cell Death Differ. **14:**1475–1485.
30. **Munro, S., and H. R. Pelham.** 1987. A C-terminal signal prevents secretion of luminal ER proteins. Cell **48:**899–907.
31. **Munro, S., and H. R. Pelham.** 1986. An Hsp70-like protein in the ER: identity with the 78 kd glucose-regulated protein and immunoglobulin heavy chain binding protein. Cell **46:**291–300.
32. **Ogawa, M., T. Miyata, K. Nakajima, K. Yagyu, M. Seike, K. Ikenaka, H. Yamamoto, and K. Mikoshiba.** 1995. The reeler gene-associated antigen on Cajal-Retzius neurons is a crucial molecule for laminar organization of cortical neurons. Neuron **14:**899–912.
33. **Ohshima, T., J. M. Ward, C. G. Huh, G. Longenecker, Veeranna, H. C. Pant, R. O. Brady, L. J. Martin, and A. B. Kulkarni.** 1996. Targeted disruption of the cyclin-dependent kinase 5 gene results in abnormal corticogenesis, neuronal pathology and perinatal death. Proc. Natl. Acad. Sci. USA **93:**11173–11178.
34. **Oyadomari, S., A. Koizumi, K. Takeda, T. Gotoh, S. Akira, E. Araki, and M. Mori.** 2002. Targeted disruption of the Chop gene delays endoplasmic reticulum stress-mediated diabetes. J. Clin. Investig. **109:**525–532.
35. **Patil, C., and P. Walter.** 2001. Intracellular signaling from the endoplasmic reticulum to the nucleus: the unfolded protein response in yeast and mammals. Curr. Opin. Cell Biol. **13:**349–355.
36. **Reimold, A. M., A. Etkin, I. Clauss, A. Perkins, D. S. Friend, J. Zhang, H. F. Horton, A. Scott, S. H. Orkin, M. C. Byrne, M. J. Grusby, and L. H. Glimcher.** 2000. An essential role in liver development for transcription factor XBP-1. Genes Dev. **14:**152–157.
37. **Reimold, A. M., N. N. Iwakoshi, J. Manis, P. Vallabhajosyula, E. Szomolanyi-Tsuda, E. M. Gravallese, D. Friend, M. J. Grusby, F. Alt, and L. H. Glimcher.** 2001. Plasma cell differentiation requires the transcription factor XBP-1. Nature **412:**300–307.
38. **Scheuner, D., B. Song, E. McEwen, C. Liu, R. Laybutt, P. Gillespie, T. Saunders, S. Bonner-Weir, and R. J. Kaufman.** 2001. Translational control is required for the unfolded protein response and in vivo glucose homeostasis. Mol. Cell **7:**1165–1176.
39. **Schroder, M., and R. J. Kaufman.** 2005. The mammalian unfolded protein response. Annu. Rev. Biochem. **74:**739–789.
40. **Sonnichsen, B., J. Fullekrug, P. N. Van, W. Diekmann, D. G. Robinson, and G. Mieskes.** 1994. Retention and retrieval: both mechanisms cooperate to maintain calreticulin in the endoplasmic reticulum. J. Cell Sci. **107:**2705–2717.
41. **Tajiri, S., S. Oyadomari, S. Yano, M. Morioka, T. Gotoh, J. I. Hamada, Y. Ushio, and M. Mori.** 2004. Ischemia-induced neuronal cell death is mediated by the endoplasmic reticulum stress pathway involving CHOP. Cell Death Differ. **11:**403–415.

42. **Taxis, C., F. Vogel, and D. H. Wolf.** 2002. ER-Golgi traffic is a prerequisite for efficient ER degradation. Mol. Biol. Cell **13**:1806–1818.
43. **Tissir, F., and A. M. Goffinet.** 2003. Reelin and brain development. Nat. Rev. Neurosci. **4**:496–505.
44. **Utsunomiya-Tate, N., K. Kubo, S. Tate, M. Kainosho, E. Katayama, K. Nakajima, and K. Mikoshiba.** 2000. Reelin molecules assemble together to form a large protein complex, which is inhibited by the function-blocking CR-50 antibody. Proc. Natl. Acad. Sci. USA **97**:9729–9734.
45. **Vashist, S., and D. T. Ng.** 2004. Misfolded proteins are sorted by a sequential checkpoint mechanism of ER quality control. J. Cell Biol. **165**:41–52.
46. **Wu, J., and R. J. Kaufman.** 2006. From acute ER stress to physiological roles of the unfolded protein response. Cell Death Differ. **13**:374–384.
47. **Yamamoto, K., R. Fujii, Y. Toyofuku, T. Saito, H. Koseki, V. W. Hsu, and T. Aoe.** 2001. The KDEL receptor mediates a retrieval mechanism that contributes to quality control at the endoplasmic reticulum. EMBO J. **20**:3082–3091.
48. **Yuasa, S., J. Kitoh, S. Oda, and K. Kawamura.** 1993. Obstructed migration of Purkinje cells in the developing cerebellum of the reeler mutant mouse. Anat. Embryol. (Berlin) **188**:317–329.
49. **Zhao, L., C. Longo-Guess, B. S. Harris, J. W. Lee, and S. L. Ackerman.** 2005. Protein accumulation and neurodegeneration in the woozy mutant mouse is caused by disruption of SIL1, a cochaperone of BiP. Nat. Genet. **37**:974–979.
50. **Zinszner, H., M. Kuroda, X. Wang, N. Batchvarova, R. T. Lightfoot, H. Remotti, J. L. Stevens, and D. Ron.** 1998. CHOP is implicated in programmed cell death in response to impaired function of the endoplasmic reticulum. Genes Dev. **12**:982–995.

MOLECULAR AND CELLULAR BIOLOGY, Feb. 2008, p. 1018–1028
0270-7306/08/$08.00+0 doi:10.1128/MCB.01136-07

Vol. 28, No. 3

Inactivation of the Polycomb Group Protein Ring1B Unveils an Antiproliferative Role in Hematopoietic Cell Expansion and Cooperation with Tumorigenesis Associated with *Ink4a* Deletion▽†

Carmela Calés,[2] Mónica Román-Trufero,[1] Leticia Pavón,[2] Iván Serrano,[2] Teresa Melgar,[1] Mitsuhiro Endoh,[3] Claudia Pérez,[4] Haruhiko Koseki,[3] and Miguel Vidal[1,3]*

Centro de Investigaciones Biológicas, Consejo Superior de Investigaciones Científicas, Ramiro de Maeztu 9, 28004 Madrid, Spain[1]; Instituto de Investigaciones Biomédicas, Universidad Autónoma de Madrid, Consejo Superior de Investigaciones Científicas, Arturo Duperier 4, 28029 Madrid, Spain[2]; Riken Research Center for Allergy and Immunology, 1-7-22 Suehiro, Tsurumi-ku, Yokohama 230-0045, Japan[3]; and Anatomy and Histopathology, Facultad de Veterinaria, Universidad de León, Campus Vegazana, 24071 León, Spain[4]

Received 26 June 2007/Returned for modification 2 August 2007/Accepted 12 November 2007

Polycomb group (PcG) proteins act as positive regulators of cell proliferation. *Ring1B* is a PcG gene essential for embryonic development, but its contribution to cell turnover in regenerating tissues is not known. Here, we have generated a conditional mouse mutant line to study the Ring1B role in adult hematopoiesis. Mutant mice developed a hypocellular bone marrow that paradoxically contained an enlarged, hyperproliferating compartment of immature cells, with an intact differentiation potential. These alterations were associated with differential upregulation of cyclin D2, which occurred in all mutant bone marrow cells, and of $p16^{Ink4a}$, observed only in the differentiated compartment. Concurrent inactivation of *Ink4a* rescued the defective proliferation of maturing cells but did not affect the hyperproliferative activity of progenitors and resulted in a shortening of the onset of lymphomas induced by *Ink4a* inactivation. These data show that Ring1B restricts the progenitors' proliferation and promotes the proliferation of their maturing progeny by selectively altering the expression pattern of cell cycle regulators along hematopoietic differentiation. The novel antiproliferative role of Ring1B's downregulation of a cell cycle activator may play an important role in the tight control of hematopoietic cell turnover.

Adult multicellular organisms have evolved cell turnover strategies adapted to the maintenance and repair of tissues. In many cases, such as the hematopoietic system, gut, skin, and brain, tissue homeostasis depends on the activity of multipotent stem cells from which derive all the cell lineages that make these tissues (17, 56). Because of the relatively small number of stem cells, their progeny undergoes an expanding but limited number of cell divisions along the differentiation process before entering the mitotically inactive state of fully mature cells. Tissue homeostasis, then, depends on an adequate balance between stem cell renewal, regulated cell proliferation, and terminal differentiation of stem cell progeny (58, 74).

The Polycomb group (PcG) of proteins are transcriptional repressors that prevent the inappropriate expression of genes that determine cell identity (4, 11). PcG gene products assemble in multimeric complexes (Polycomb repressing complexes [PRC]) whose transcriptional activity is associated to their role as chromatin modifiers (64). PRC are compositionally diverse, but depending on which of two sets of core subunits they contain, they are designated type PRC1 or PRC2 (40). Histone H2AK119 monoubiquitylation depends on the RING finger E3 ligases of PRC1 complexes (10, 73), whereas histone H3K27 trimethylation is carried out by PRC2 complexes (12, 18, 34, 46). Well known as developmental regulators (57), PcG genes also play important roles in cell proliferation control (41, 52). Murine models of loss of function of PcG genes encoding PRC1 subunits show reduced size and hypocellularity of hematopoietic organs (1, 15, 69, 70) and also, in some cases (Bmi1) of brain structures (71), indicating that PcG complexes are positive regulators of cell proliferation. The upregulation of PcG products observed in a wide variety of tumors (54, 68) and their cooperation in oncogene-induced tumorigenesis (27) further support a role for PcG complexes as promoters of proliferation. Exceptionally, inactivation of the PRC2 subunit Eed resulted in enlarged hematopoietic compartments (36). These alterations are due, at least in part, to PcG-mediated repression of the *Ink4a/Cdkn2a* locus, which encodes the tumor suppressors $p16^{Ink4a}$ and $p19^{Arf}$. Loss of function of PRC1 proteins, and Bmi1 in particular, results in premature senescence of hematopoietic and neuronal stem cells (28, 37, 44, 48, 49, 51). PcG complexes also promote expansion of maturing cells by preventing senescence and apoptosis, although the contribution of each of these mechanisms varies depending on the particular tissue and the PcG protein (9, 14, 38, 45).

Ring1B and its paralog Ring1A are the RING finger E3 ligases that monoubiquitylate H2A (20, 73). They associate directly with Bmi1, Mel18, M33, and Phc1, forming the core of

* Corresponding author. Mailing address: Developmental and Cell Biology, Centro de Investigaciones Biológicas, Ramiro de Maeztu, 9, 28040 Madrid, Spain. Phone: 34 91 837 3112, ext. 4383. Fax: 34 91536 0432. E-mail: mvidal@cib.csic.es.

† Supplemental material for this article may be found at http://mcb.asm.org/.

▽ Published ahead of print on 26 November 2007.

PRC1 complex(es) (25, 39, 63). The contribution of Ring1A and Ring1B to cell turnover of renewing tissues is not known. Constitutive inactivation of Ring1A results in fertile mice with no overt phenotypes (19), whereas inactivation of Ring1B leads to embryonic lethality due to defective gastrulation (72). Considering that Ring1B expression in the adult hematopoietic compartment is detected in all differentiation stages, from the hematopoietic stem cells (HSCs) and their immature descendants (29), we sought to address the role of Ring1B in adult hematopoiesis using a conditional mutant mouse line. We find that Ring1B inactivation results in a reduction of total bone marrow cells and, at the same time, an enlargement of the immature cell compartment. We also show that the alterations in the size of bone marrow cell populations are due to cell proliferation defects caused by upregulation of components of the cell cycle machinery that act as activators (cyclin D2) or inhibitors ($p16^{Ink4a}$) of proliferation in a differentiation stage-dependent manner. Finally, we observed premature development of lymphomas in compound *Ring1B;Ink4a* mutant mice that suggests an important role for Ring1B in controlling the expansion of progenitor cells in adult hematopoiesis.

MATERIALS AND METHODS

Mice, genotyping, and conditional inactivation of *Ring1B*. *Ring1B* genomic sequences for the targeting vector were generated from a partial genomic clone isolated from a mouse 129SVJ Lambda FIX II phage library (Stratagene) probed with a *Ring1B* cDNA. The 5′ arm of the targeting vector was a 4,680-kb EcoRI-BstNI fragment corresponding to sequences located 4,464 bp 5′ from the intron 2-exon 3 junction, and the 3′ arm was a 5,286-bp BstNI-EcoRI fragment encompassing sequences up to 97 bp 3′ of the exon 5-intron 5 boundary. They were subcloned into pPGKneo2loxDTA plasmid (67), which contains a phosphoglycerol kinase promoter-*neomycin* resistance gene cassette flanked by two *loxP* sites and a phosphoglycerol kinase-*diphteria toxin* gene cassette (see Fig. S1A in the supplemental material). The 5′ arm was modified by inserting an oligonucleotide containing a *loxP* sequence and a BglII site at the AvrII site 197 bp 5′ from the intron 1-exon 2 junction using a PCR strategy. The targeting construct was linearized and electroporated into 2×10^7 mouse R1 embryonic stem (ES) cells. Colonies surviving the G418 selection were transferred into duplicated 48-well plates, which were used to prepare frozen stocks of the ES cell colonies and to isolate genomic DNA, respectively. The targeted allele was identified by Southern blotting using probes external to the targeting vector (see Fig. S1A in the supplemental material). Two $Ring1B^{flox/+}$ (hereafter, $Ring1B^{f/+}$) ES clones were aggregated with morulae obtained from C57Bl10 mice, and the resulting chimeric males were mated to C57Bl10 mice, and heterozygous animals were identified by Southern blotting. For routine genotyping, genomic DNA was analyzed by using a three-primer PCR (see Fig. S1A in the supplemental material).

For in vivo conditional inactivation, $Ring1B^{flox/flox}$ (hereafter, $Ring1B^{f/f}$) mice were crossed with *MxCre* transgenic mice (33). *MxCre* expression was induced by intraperitoneally injecting 250 μg of polyinosine-polycytidine (pIpC; Pharmacia) on three alternate days in 6- to 12-week-old mice. "Ex vivo" conditional inactivation of *Ring1B* was carried out on cells obtained from mice generated by crossing $Ring1B^{f/f}$ mice with $RERT^{tm}$ mice, a mouse line in which an *IRES-CreERT2* (tamoxifen-inducible Cre) cassette was knocked in into the 3′ untranslated region of the RNA *polII* (*Polr2a*) gene (43), to obtain $Ring1B^{f/f}$; $RERT^{tm/tm}$ mice (here termed $Ring1B^{f/f}$ *CreERT2*). Translocation of Cre-ERT2 to cell nuclei and *loxP* recombination were achieved by adding to the cultures 4′-hydroxy tamoxifen ([4-HT] 0.4 μM final concentration; Sigma) or vehicle (+4-HT and −4-HT cultures, respectively).

Compound $Ring1B^{f/f}$; $Ink4a^{-/-}$ mice were obtained by crossing $Ring1B^{f/f}$ mice with the $Ink4a^{-/-}$ mouse line (65). Genotyping of the *Ink4a* allele was done by Southern blotting as described previously (65). All mouse procedures were institutionally approved and were in accordance with national and European regulations.

Cell counting and blood analysis. Bone marrow cells were flushed out of both femurs with phosphate-buffered saline (PBS) containing 2% fetal calf serum (PBS–2% FCS) under sterile conditions. Spleens and thymi were disrupted in a Dounce homogenizer (loose pestle) in PBS–2% FCS. Cells were counted in a hemocytometer.

Blood was obtained by heart puncture immediately after mice were sacrificed. Blood counts were mostly performed by manual counting on a hemocytometer or automatically using an Abacus (Diatron) hematological analyzer. Manual counting of white blood cells was carried out after erythrocytic lysis.

Immunophenotyping and cell separation. Single-cell suspensions were washed with PBS and resuspended in cold washing solution (PBS–2% FCS–0.1% sodium azide). The appropriate antibodies were then added, and cells were labeled for 20 min at 4°C. After a washing step, cells labeled with biotin-conjugated antibodies were further incubated with streptavidin conjugated to phycoerythrin (PE) or peridinin chlorophyll protein-Cy5.5. Samples were acquired in a FACScan fluorescence-activated cell sorter (FACS) instrument with CellQuest software or a FACSCanto with Diva software, all from Becton Dickinson. The antibodies that were used were as follows: c-Kit conjugated to fluorescein isothiocyanate (FITC), biotin, or allophycocyanin (for analysis); Sca-1, Gr-1, CD41, and B220 conjugated to FITC or biotin; Mac-1, CD3, and Ter119 conjugated to biotin; CD34 conjugated to FITC; FcγR and CD19 conjugated to PE. All antibodies were purchased from BD Biosciences.

For common myeloid progenitor (CMP) sorting, isolated colonies with immature phenotype were pooled, immunomagnetically depleted of Lin^+ cells, and labeled with anti-c-Kit-allophycocyanin -, anti-CD34-FITC-, and anti-FcγR-PE-conjugated antibodies and sorted on the $c\text{-}Kit^+/CD34^+/Fc\gamma R^{lo}$ gate in a FACS Vantage sorter equipped with a Diva system (BD Biosciences), set to render the highest purity. Immunomagnetic cell isolation was done using a Lineage Cell Depletion kit and LD columns together with a QuadroMACS separation unit from Miltenyi Biotec. Hematopoietic cell subpopulations for Ring1B expression analysis were isolated by cell sorting as described previously (30), using $Mac1^+$ $Gr1^{lo}$ for monocytic and $Mac1^+$ $Gr1^{high}$ for granulocytic precursors, respectively, in a FACS Vantage sorter (BD Biosciences).

In vitro colony forming assays. Myeloid and pre-B-cell colony plating assays were performed in cytokine-supplemented methylcellulose-based medium M3434 and M3630 (StemCell Technologies), seeding total bone marrow in duplicate (2×10^5 or 2×10^4 cells/35-mm dish for pre-B-cell and myeloid assays, respectively). For assays of isolated progenitors, 500 Lin^- cells were used per plate. Myeloid cultures were scored for colony formation and morphologically analyzed at day +12 unless otherwise specified. Pre-B-cell and immature myeloid colonies were systematically scored at day +8 and day +7 after seeding, respectively. Serial replating, using equal numbers of cells, was performed 10 days after plating.

Cell proliferation, cell division, and apoptosis assays. Bone marrow or isolated Lin^- cells were cultured in 24-well plates containing Iscove's modified Dulbecco's medium–10% FCS medium plus 20 or 50 ng/ml of recombinant murine interleukin-3 (IL-3) or recombinant human IL-6, respectively (Peprotech). Recombination in cultured cells was achieved by adding 4-HT (0.4 μM; Sigma) or vehicle, where indicated. Lin^- cells cultures also contained 100 ng/ml of recombinant human stem cell factor (Peprotech). Viable cells were counted by trypan blue exclusion in a hemocytometer.

Bromodeoxyuridine (BrdU) incorporation was assessed by adding the nucleotide precursor analog to the culture medium at a final concentration of 10 μM. After 18 h labeled cells were determined with a fluorochrome-conjugated anti-BrdU antibody (FITC BrdU flow kit; BD-Pharmingen) and analyzed by flow cytometry in a FACScan cytometer equipped with CellQuest software (BD Biosciences). For cell division assays, cells were labeled with 2 μM carboxyfluorescein diacetate succinimidyl ester (CFDA-SE) and handled as indicated by the manufacturer (Invitrogen). Cell-associated fluorescence was analyzed by flow cytometry 18 h later. To determine the fluorescence associated to cells before division, two aliquots were removed: one was analyzed immediately, and the second was kept at 4°C to match the analysis conditions. An FITC-conjugated recombinant human annexin V kit (Bender Medsystems) was used to stain apoptotic cells prior to flow cytometry analysis.

Western blotting analysis. Cells were lysed in radioimmunoprecipitation assay buffer (10 mM Tris-HCl, pH 7.2, 150 mM NaCl, 1% TX-100, 0.1% sodium dodecyl sulfate, 1% deoxycholate, 5 mM EDTA, 20 mM NaF, 100 μM orthovanadate, and protease inhibitors) for 30 min on ice. Cell lysates were cleared of debris by centrifugation at 15,000 × *g* for 15 min, aliquoted, snap-frozen, and kept at −70°C until used. Thirty micrograms of total protein was subjected to sodium dodecyl sulfate-polyacrylamide gel electrophoresis and transferred to BioTrace polyvinylidene difluoride membranes (Pall Corporation) for 1 h at 2 mA/cm^2 on a semidry transfer apparatus (Amersham). Ponceau staining was routinely performed on membranes, and digital photographs were taken in order to record a sample loading control. After being blocked in Tris-buffered saline containing 0.1% Tween 20 and 5% nonfat dry milk, filters were incubated

overnight at 4°C with the following antibodies: anti-Ring1B (63), anti-$p16^{Ink4a}$ (M-156; Santa Cruz), anti-cyclin D2 (M-20; Santa Cruz), anti-cyclin D3 (C-16; Santa Cruz), anti-$p27^{kip1}$ (clone 57; Transduction Laboratories), anti-cdc6 (Ab-3; Oncogene), anti-$p57^{kip2}$ (KP-39; Sigma), anti-cyclin A (H-432; Santa Cruz), anti $p19^{Arf}$ (ab80; Abcam). After a washing step and incubation with horseradish peroxidase-conjugated secondary antibodies (Dako), signals were detected using an enhanced chemiluminescence system (Pierce).

Histopathology and immunohistochemistry. Normal and tumor tissue samples were fixed in 10% neutral-buffered formalin for 24 h. After dehydration and paraffin wax embedding, 3-μm sections were prepared and stained with hematoxylin and eosin. For immunohistochemical analysis, sections were mounted on poly-L-lysine-coated slides, and anti-Pax5 antibodies were detected by the avidin-biotin-peroxidase complex method (Peroxidase Elite, Vectastain, and ABC kit; Vector Laboratories).

Quantitative reverse transcription-PCR expression analysis. RNA was isolated from sorted hematopoietic cell populations using an RNeasy kit (Qiagen). Random-primed cDNA was generated using a Superscript III First Strand reverse transcription kit (Invitrogen). Triplicate reactions of cDNA amplification were performed in Sybr Premix Ex *Taq* (Takara) and analyzed using a 7900HT Fast Real-Time PCR System (Applied Biosystems). Relative mRNA normalized to acidic ribosomal phosphoprotein mRNA levels was determined using the comparative cycle threshold ($\Delta\Delta C_T$) method. The following sets of primers were used: for Ring1B, TTGACATAGAATGGGACAGC (forward) and GTCAGC AGAAAGTCTTGTGG (reverse); for acidic ribosomal phosphoprotein, CGAC CTGGAAGTCCAACTAC (forward) and ATCTGCTGCATCTGCTTG (reverse).

ChIP. Lin^- and Lin^+ bone marrow cells were processed for chromatin immunoprecipitation (ChIP) assays using anti-trimethylated H3K27 (Upstate), anti-Ring1B (3), and anti-Bmi1 (21) antibodies. Immunoprecipitated DNA was amplified using the primer pair TTGCCCTGAATATAGCATGA and TCATG CTATATTCAGGGCAA or the pair CGATCCTTTAGCGCTGTTTC and CA CACTCTGCTCCTGACCTG that span 271 bp and 201 bp in the murine $p16^{Ink4a}$ gene promoter area, respectively.

Statistical analyses. Values are expressed as means ± standard deviation (SD). Data sets were compared using a two-tailed Student's *t* test, and differences were considered significant for *P* values of <0.05.

RESULTS

Loss of *Ring1B* leads to concurrent bone marrow hypocellularity and enlarged immature cell compartments. Ring1B mRNA expression was found to be ubiquitous in hematopoietic cells, from the most primitive HSC and its derived progenitors (CMP and common lymphoid progenitor) through more committed but still immature bivalent progenitors (granulo-monocytic progenitors [GMPs] and megakaryo-erythrocytic progenitors [MEP]) and the most mature myeloid and lymphoid cells (Fig. 1A). To study the function of Ring1B during adult hematopoiesis, we crossed a pIpC-inducible MxCre mouse line that expresses the Cre recombinase in the hematopoietic compartment (33) with a conditional *Ring1B*$^{f/f}$ mouse line (Fig. 1B) to produce *Ring1B*$^{f/f}$; *MxCre* mice and their *MxCre*-negative littermate controls. Six- to 12-week-old mice were treated with pIpC and sacrificed 4 weeks later. The treatment resulted in efficient deletion of alleles flanked by *loxP* sites (see Fig. S1A in the supplemental material) and loss of Ring1B protein in the bone marrow (Fig. 1B).

Examination of circulating blood cells and secondary hematopoietic organs (spleen and thymus) of *MxCre*-positive and *MxCre*-negative mice showed only mild, but consistent, reduction of erythrocytes and splenocytes in most mutant animals and a few thrombocytotic individuals (see Fig. S2A and B in the supplemental material). Immunophenotypic analysis of bone marrow cells showed no remarkable differences in lineage composition between normal and mutant mice, except for a slight decrease of mutant lymphoid B cells (see Fig. S2C in the supplemental material). A relevant difference, however, was seen in total bone marrow cell numbers, which were reduced upon *Ring1B* ablation by nearly one-third ($P = 0.001$) (Fig. 1C). In contrast, the progenitor compartment (minority cells lacking lineage differentiation markers, i.e., Lin^- cells) was enlarged in mutant bone marrow (Fig. 1D). The HSC-enriched subpopulation (Lin^- cells that simultaneously express c-Kit and Sca-1 markers) was also larger than that of Ring1B-expressing cells (Fig. 1E). Thus, *Ring1B* ablation resulted in concurrent hypocellularity of the mature bone marrow and an increased number of progenitor cells, with no apparent alterations in lineage specification.

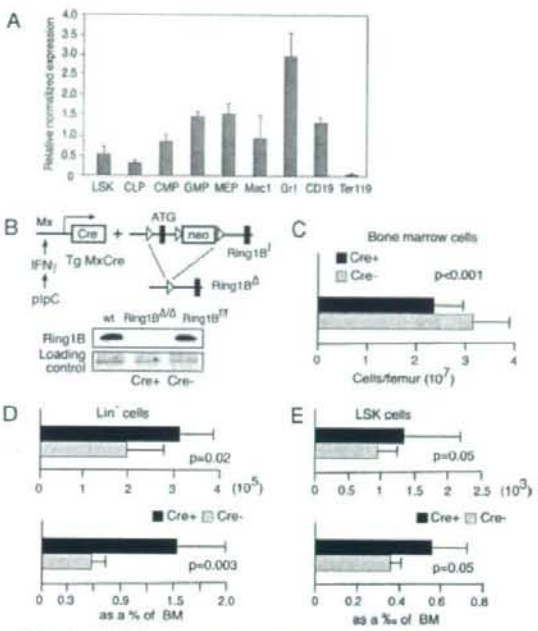

FIG. 1. Conditional targeting of *Ring1B* and analysis of *Ring1B*-deficient bone marrow cells. (A) Analysis by quantitative reverse transcription-PCR of the expression levels of Ring1B in the indicated subpopulations of hematopoietic progenitors and their maturing progeny. LSK, $Lin^-Sca\text{-}1^+c\text{-}Kit^+$ cells, corresponding to long- and short-term HSCs; CLP, common lymphoid progenitors; Mac1, monocytic precursors; Gr1, granulocytic precursors; CD19, B-cell precursors; Ter119, erythocytic precursors. Each value has been normalized for acidic ribosomal phosphoprotein expression levels. (B) Schematic representation of strategy used to ablate *Ring1B* in vivo and results of Ring1B detection by Western blotting in bone marrow from *Ring1B*$^{f/f}$ mice and from mice lacking the *Ring1B* locus (*Ring1B*$^{\Delta/\Delta}$). (C) Total bone marrow cell count from *Ring1B*$^{f/f}$ ($n = 20$; Cre^-) and *Ring1B*$^{\Delta/\Delta}$ ($n = 20$; Cre^+) mice. (D) Absolute (top) and relative (bottom) numbers of bone marrow cells lacking lineage markers (Lin^- population, corresponding to HSC and all progenitor cells) from *Ring1B*$^{f/f}$ ($n = 12$; Cre^-) and *Ring1B*$^{\Delta/\Delta}$ ($n = 12$; Cre^+) mice. (E) Absolute (top) and relative (bottom) numbers of LSK population (corresponding to long- and short-term HSCs) from control ($n = 10$; Cre^-) and mutant ($n = 10$; Cre^+) immunomagnetically isolated Lin^- cells. BM, bone marrow; IFN-γ, gamma interferon; wt, wild type; Tg, transgenic.

Cell-autonomous increase of *Ring1B*-deficient myeloid clonogenic cells. Clonogenic assays were employed to determine

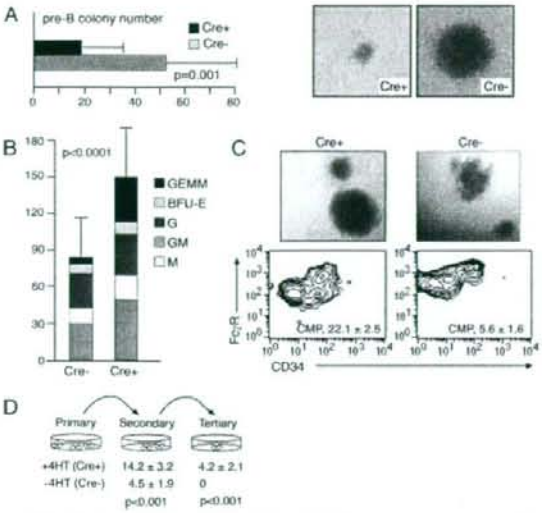

FIG. 2. Clonogenic assays of *Ring1B*-deficient bone marrow cells. (A) Impaired pre-B-cell colony formation in mice in which the *Ring1B* locus has been excised as a result of the expression of MxCre. Colonies generated per 5×10^5 bone marrow cells from mutant ($n = 14$; Cre^+) and control ($n = 12$; Cre^-) mice. At right are images of representative colonies at day +8 of culture. (B) Increased myeloid clonogenic activity in $MxCre^+$ (excised *Ring1B*) mice ($n = 14$; Cre^+) compared to $MxCre^-$ (nonexcised *Ring1B*) mice ($n = 16$; Cre^-). Bar segments represent the average absolute number (CFU) of the various colony types: unilineage monocytic (M), granulocytic(G), and erythrocytic (BFU-E) and bilineage granulo-monocytic (GM) and GEMM (mixed) colonies. (C) Myeloid colonies. At top are photographs of representative individual immature colonies picked at day +7 of culture; at bottom are contour plots of the flow cytometry analysis of these colonies showing the myeloid progenitors MEPs, GMPs, and CMPs identified as $CD34^-$ $FcγR^{lo}$ (lower left lobe), $CD34^+$ $FcγR^+$ (upper right lobe), and $CD34^+$ $FcγR^{lo}$ (lower right lobe; almost absent in control Cre^- colonies), respectively. A representative experiment (out of three) is shown, indicating the CMP relative content value ± SD. (D) Replicating assay of ex vivo *Ring1B*-excised bone marrow cells. The results are shown as the mean ± SD ($n = 6$) of the total number of secondary and tertiary colonies generated from identical numbers of pooled primary control (−4-HT) and mutant (+4-HT) myeloid colonies.

the abundance of cells (CFU) able to expand and give rise to differentiated progeny in vitro. These include primitive, multilineage progenitors and immediate unilineage precursors that give rise to characteristic, morphologically distinguishable colonies. For lymphoid cells, clonogenic assays in the presence of IL-7 revealed a severe reduction in the number and size of *Ring1B*-deficient pre-B-cell colonies (Fig. 2A). On the other hand, ablation of *Ring1B* resulted in an almost twofold increase of myeloid CFU (Fig. 2B). Whereas all types of supported CFU were represented, their relative proportions were altered, particularly the mixed granulo-mono-erythromegakaryocitic (GEMM) colonies (sixfold increase; $P < 0.0001$) (Fig. 2B) originated from the most immature progenitors. The GEMM colonies derived from blast-like cell clusters, which in mutant bone marrow cultures appeared invariably denser (Fig. 2C, top) and also contained a higher proportion of the primitive CMP (fivefold increase; $P = 0.05$) (Fig. 2C, bottom). We conclude that Ring1B clearly affected both the size and clonogenic activity of the progenitors' compartment.

Since extrinsic signals affect hematopoiesis, we aimed to determine the cell-autonomous contribution to the above alterations. To do this, we devised an ex vivo *Ring1B* inactivation system that used bone marrow cells from *Ring1B*$^{f/f}$; *Cre-ERT2* mice. These were obtained by crossing the conditional *Ring1B*$^{f/f}$ mouse line with a *RERT*^{ert} mouse deleter line (*Cre-ERT2::Polr2a* [43]) (see Fig. S3A in the supplemental material). The mouse deleter line ubiquitously expresses a tamoxifen (4-HT)-inducible fusion protein between the Cre recombinase and a mutated ligand binding domain of the human estrogen receptor. Bone marrow cells from these mice were cultured in parallel in the absence (Cre^-) and in the presence (Cre^+) of 4-HT to generate control and *Ring1B*-deleted cells, respectively. Efficient *Ring1B* ablation was achieved 2 days after 4-HT treatment (see Fig. S3B in the supplemental material). As seen above for in vivo *Ring1B*-inactivated bone marrow cells (Fig. 2A and B), 4-HT treatment resulted in a reduction of pre-B-cell colonies, an increase in total Lin^- cells, and a larger number of myeloid CFU (see Fig. S3C to E in the supplemental material). Consistent with this, mutant progenitors (+4-HT; Cre^+) yielded more secondary and tertiary colonies in a replicating assay than control progenitors (−4-HT; Cre^-), indicating a higher self-renewal rate of *Ring1B*-deficient cells (Fig. 2D). These results indicate that alteration of immature cell populations and of their clonogenic activities are mostly due to a cell-autonomous defect resulting from the ablation of *Ring1B*.

***Ring1B* inactivation enhances the proliferative rate of myeloid progenitors.** We used ex vivo inactivation of *Ring1B* to investigate whether differences in cell proliferation rate, apoptosis, or cell differentiation could account for the accumulation of *Ring1B*-deficient primitive hematopoietic cells. Pulse labeling of Lin^- cells with BrdU demonstrated that more cells incorporated BrdU in 4-HT-treated (Cre^+) than in nontreated (Cre^-) cultures (Fig. 3A). We also used CFDA-SE fluorescence decay as an additional test of the cell division rate. This assay is based on the dilution of the fluorescent dye resulting from its equal distribution among daughter cells upon cell division. As shown in Fig. 3B, nearly all *Ring1B*-deficient Lin^- cells had completed one cell cycle at the same point when 30% of the *Ring1B*-expressing Lin^- cells still remained undivided. Under these culture conditions, annexin V labeling (an indicator of apoptosis) showed no differences between treated and nontreated cultures (Fig. 3C). These results indicate that the enlargement of the mutant Lin^- compartment is due to an increase in the cell proliferation rate provoked by the loss of *Ring1B*.

Although the representation of the various lineages in bone marrow and circulating cells in *Ring1B* mutant mice suggested that no major alterations in differentiation were occurring, we further tested this by immunophenotyping cells generated in methylcellulose cultures of Lin^- cells. As seen in Fig. 3D, levels of Gr-1, Mac-1, and CD-41 lineage markers (specific for granulocytes, monocytes, and megakaryocytes, respectively) showed no differences between cultures from *Ring1B*-deleted and nondeleted Lin^- cells. Moreover, FACS-sorted mutant CMPs retained the ability to give rise in vitro to more mature progeny, MEPs and GMPs (Fig. 3E). Together, these data

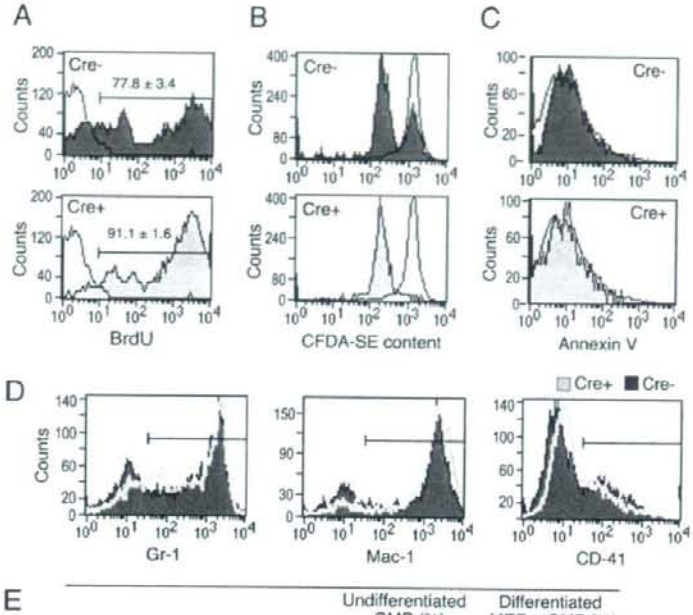

E

	Undifferentiated CMP (%)	Differentiated MEP + GMP (%)
Sorted CMP	>99.0	<1.0
d +7 myeloid differentiation (Exp. 1)	26.5	57.0
d +7 myeloid differentiation (Exp. 2)	36.2	53.8

FIG. 3. Increased proliferation of Ring1B-deficient progenitors. (A to C) Proliferation and apoptosis of Lin$^-$ cells isolated from *Ring1B*$^{fl/fl}$; *Cre-ERT2* bone marrow cells in the absence (Cre$^-$; top) or the presence (Cre$^+$; bottom) of 4-HT. (A) Solid plots correspond to cells labeled with anti-BrdU antibodies. Overlaid empty plots correspond to cells labeled with isotype-matching FITC antibody to define the BrdU-negative population. Proliferating, BrdU-positive cells (indicated by the bar) are shown as the mean ± SD of two duplicate, independent experiments. (B) CFDA-SE fluorescence content of mutant (+4-HT; Cre$^+$) (bottom) or control (−4-HT; Cre$^-$) (top) Lin$^-$ cells, 18 h after immunoseparation and fluorescent dye incubation. The empty histogram shows CFDA-SE cell content immediately after dye loading. (C) FITC-conjugated annexin V labeling of propidium iodide-impermeable viable Lin$^-$ cells cultured with (Cre$^+$; bottom) or without (Cre$^-$; top) 4-HT. The overlaid empty histogram corresponds to cells treated under the same conditions but with no added annexin V. (D) Expression of lineage markers in cells from mutant (light empty plots) and control (dark solid plots) myeloid colonies harvested at day +8. Gr-1, Mac-1, and CD41 markers stain mature cells of the granulocytic, monocytic, and megakaryocytic lineages, respectively. Bars indicate positively labeled cells. (E) Mutant CMPs retain their differentiation potential. Sorted mutant CMPs (Lin$^-$ c-Kit$^+$ CD34$^+$ FcγR^{lo}) cells were seeded into myeloid differentiation medium and individual colonies appearing at day +7 (d +7)were labeled with antibodies to c-Kit, CD34, and FcγR to determine MEP, CMP, and GMP content as indicated in the legend of Fig. 2.

strongly suggest that the accumulation of early progenitor cells resulting from *Ring1B* inactivation is mostly due to an enhanced proliferation rate of myeloid progenitors and not to reduced apoptosis or impairment of their differentiating ability.

Ring1B negatively regulates cyclin D2 and p16^{Ink4a}. After establishing the role of Ring1B in proliferation of hematopoietic cells, we began to study the underlying mechanism(s) by analyzing protein expression levels of known cell cycle regulators. The rate of cell proliferation in mammalian cells is determined mainly in the G_1 phase of the cell cycle by the specific activation of cyclin-dependent kinases, which are in turn negatively regulated by two families of cyclin-dependent kinase inhibitors (CKIs) (66). First, we compared total bone marrow cell extracts from control *MxCre*-negative and in vivo deleted *Ring1B* (*MxCre* positive) mice. Western blot analysis showed increased levels of cyclin D2 (Fig. 4A) and also of the cell cycle progression indicator cyclin A (see Fig. S4A in the supplemental material) in extracts from *Ring1B*-deficient cells. Also, levels of the CKI p27 appeared slightly higher in mutant cells (see Fig. S4 in the supplemental material). However, the most prominent difference was observed for the levels of p16^{Ink4a}, another CKI which, while undetectable in extracts from nondeleted cells, gave a strong signal in *Ring1B*-deficient cell extracts (Fig. 4A). No signals were detected for cdc6, a component of the replication licensing machinery, the CKI p57, or p19^{Arf} in any of the extracts (see Fig. S4A in the supplemental material).

Since the most immature cells (i.e., HSCs and progenitors) represent only a minor contribution to total bone marrow cells, we performed Western blot analysis on mutant and control Lin$^-$ cells (Fig. 3B). In contrast to whole bone marrow, the expression pattern of cell cycle regulators in mutant Lin$^-$ cells showed an upregulation of proliferation activators cyclin D2

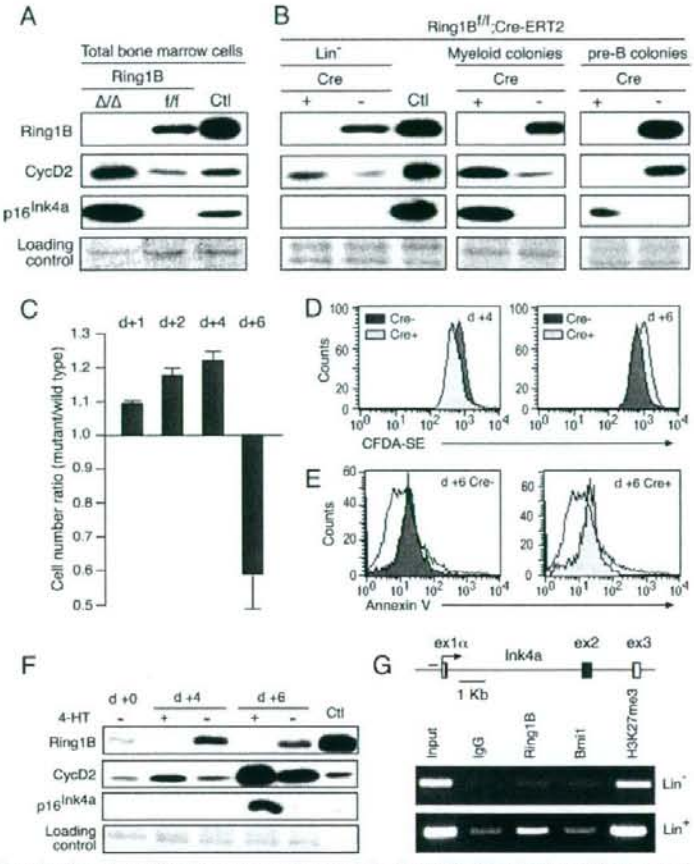

FIG. 4. Cell cycle regulator levels and proliferation rate are differentially affected by Ring1B along differentiation. (A and B) Representative Western blots (3 to 15 independent experiments) from the indicated extracts. (A) Bone marrow extracts from mice in which the *Ring1B* locus has been excised as a result of the expression of MxCre (Δ/Δ; Cre^+) and from *Ring1B*$^{f/f}$ (f/f; Cre^-) mice. (B) Blots at left are extracts from Lin^- cells immunomagnetically isolated from 4-HT-treated or untreated *Ring1B*$^{f/f}$; *Cre-ERT2* bone marrow cells cultured for 48 h. Blots of extracts from myeloid colonies harvested after culturing Lin^- cells for 8 days in methylcellulose medium without or with 4-HT are shown in the middle. At right are blots of extracts from pooled pre-B-cell colonies grown after 8-day cultures of *Ring1B*$^{f/f}$ and *Ring1B*-deficient bone marrow cells. Ctl, extracts from mouse erythroleukemia cells; +, with 4-HT treatment; −, without 4-HT treatment. In panels A and B, Ponceau red-stained membranes were used as a loading control. (C to F) Isolated Lin^- cells were cultured in suspension for the indicated times in differentiation medium containing stem cell factor, IL-3, and IL-6 in the presence (+) or absence (−) of 4-HT. (C) Differential accumulation of mutant and control cells with time in culture. Bars represent the average ratio of the percentage of mutant to control cells, considering the value of control cells as 1. (D) Switch in the values of CFDA-SE fluorescence of cells in cultures in which the *Ring1B* locus has been excised as a result of 4-HT treatment (Cre^+) and in untreated (nonexcised *Ring1B*; Cre^-) cultures at the indicated times. (E) FITC-conjugated annexin V labeling of propidium iodide-impermeable viable cells present in day +6 cells cultured with (right) or without (left) 4-HT. Overlaid empty histogram corresponds to cells treated under the same conditions but with no added annexin V. (F) Western blot analysis of cell extracts obtained from cells cultured in the presence (+) or the absence (−) of 4-HT for the indicated times. Day +0 corresponds to extracts of Lin^- cells isolated from the bone marrow of *Ring1B*$^{f/f}$; *Cre-ERT2* mice at the time of sacrifice. Controls and loading control are as described in panels A and B. (G) *Ink4a* promoter occupancy by Ring1B and Bmi1 in progenitors and maturing hematopoietic cells. At top is a schematic representation of the *p16*^{Ink4a} gene locus shows exons and coding (filled) sequences and the amplicon used for ChIP assays. Lin^- and Lin^+ cell populations were immunomagnetically isolated from bone marrow and chromatin analyzed using the indicated antibodies (bottom). Ex, exon; H3K27me3, trimethylated H3K27; IgG, immunoglobulin G; d, day.

(Fig. 4B, left), cyclin A, and cdc6 (see Fig. S4A in the supplemental material) with a concomitant absence of proliferation inhibitors p16^{Ink4a} (Fig. 4B, left), p27, and p57 (see Fig. S4A in the supplemental material). However, the analysis of colonies harvested from Lin^- cell methylcellulose cultures at day 8 showed a sustained upregulation of cyclin D2 together with a dramatic increase of p16^{Ink4a} levels in maturing *Ring1B*-deficient cells only (Fig. 4B, middle panel), thus resembling the expression pattern seen in unfractionated bone marrow cells. A similar upregulation of p16^{Ink4a} levels was observed in extracts from cultured mutant pre-B cells (Fig. 4B, right). Only cyclin D3, which is needed for the expansion of pre-B cells

(13), was detected in these cells, and its expression was hardly affected by the lack of Ring1B in either pre-B cells or myeloid cells (see Fig. S4C in the supplemental material), suggesting that the effect on cyclin D2 is specific. Modest increases in p27 and p57 levels were also observed in maturing mutant cells (see Fig. S4B in the supplemental material). These data show that *Ring1B* inactivation alters the expression pattern of cell cycle regulators in differentiating cells and suggest that the resulting populations of mature and immature cells are endowed with reduced and enhanced proliferation rates, respectively.

We investigated these cell populations by using liquid cultures of ex vivo *Ring1B*-ablated Lin$^-$ cells under conditions that recapitulate the differentiation events occurring in normal myelopoiesis. Initially after treatment, the relative accumulation of cells was faster in mutant (+4-HT; Cre$^+$) than in control (−4-HT; Cre$^-$) cultures (Fig. 4C). However, by day 6 after treatment, this ratio was inverted, and Ring1B-expressing cultures contained more cells than those of *Ring1B*-deficient cells. Analysis of CFDA-SE fluorescence decay confirmed the inversion of cell division rates between days 4 and 6 after 4-HT (Fig. 4D) treatment. The lower accumulation of mutant cells did not result from increased cell death, as determined by annexin V staining (Fig. 4E). Instead, the late upregulation of p16^{Ink4a}, detected only by day 6 after treatment (Fig. 4F), correlated with the switch in proliferation rate. This contrasted with the prompt upregulation of the proliferation promoter cyclin D2 in mutant cultures (Fig. 4F), which, in the absence of the inhibitor p16^{Ink4a}, would explain the enhanced proliferation observed before day +6. A possible explanation for the differential regulation of p16^{Ink4a} in immature versus mature cells may be related to the decreasing levels of Bmi1 during hematopoietic differentiation (26), which would ensure p16^{Ink4a} silencing in progenitors, even in the absence of Ring1B. We tested this by analyzing promoter occupancy at the *Ink4a* locus in ChIP assays and found that whereas Ring1B was detected in both immature Lin$^-$ and maturing Lin$^+$ cells, Bmi1 was seen associated predominantly in the immature compartment (Fig. 4G).

Collectively, these results show that through the balanced expression of positive and negative cell cycle regulators, Ring1B controls the expansion of differentiating hematopoietic cells both by restricting proliferation of progenitors and by contributing to their expansion during maturation.

Ink4a deficiency rescues only the expansion defects of Ring1B-deficient hematopoietic cells. Given the correlation seen between p16^{Ink4a} upregulation and proliferation inhibition in maturing ex vivo *Ring1B*-deleted cells, the overall decrease of bone marrow cells associated with *Ring1B* inactivation could be explained by similar mechanisms. To test this hypothesis, we crossed *Ring1B$^{f/f}$*; *MxCre* and *Ring1B$^{f/f}$* mice with a mouse line carrying an *Ink4a* null mutation which does not express either p16^{Ink4a} or p19^{Arf} (65). Bone marrow analysis after pIpC-induced *Ring1B* ablation showed that inactivation of the *Ink4a* locus abolished the differences in cellularities of bone marrow and spleen observed in single *Ring1B*-deficient cells (Fig. 5A). Furthermore, the severe reduction of pre-B-cell colonies associated with *Ring1B* inactivation was not observed in cultures of bone marrow cells that were also deficient in *Ink4a*, which showed even a further increase in the number and size of pre-B-cell CFU (Fig. 5B). In contrast, the increased

A

	Cre-	Cre+	
Bone marrow cells (10^6)	15.9 ± 3.8	19.6 ± 4.7	p= 0.15
Spleen cells (10^7)	8.7 ± 0.7	9.2 ±1.0	p= 0.27
Cultured Lin$^+$ cells (10^5)	1.5 ± 0.1	1.8 ± 0.4	p= 0.20

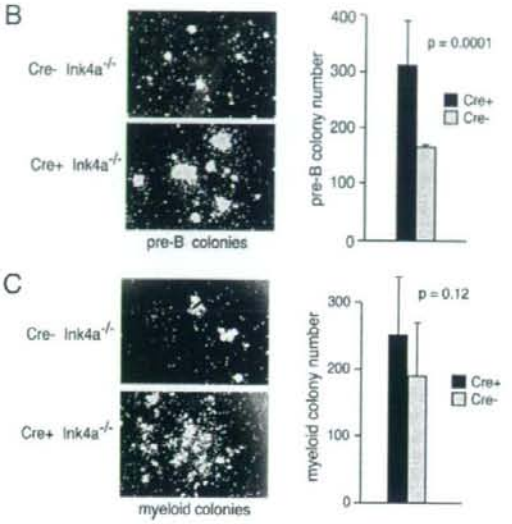

FIG. 5. *Ink4a* and *Ring1B* genetic interaction: *Ink4a* inactivation rescues impaired proliferation of *Ring1B*-deficient (*Ring1B$^{\Delta/\Delta}$*) maturing cells. (A) Total or fractionated Lin$^-$ bone marrow and total spleen cell number from *Ring1B$^{f/f}$*; *Ink4a$^{-/-}$* (n = 6) and *Ring1B$^{\Delta/\Delta}$*; *Ink4a$^{-/-}$* (n = 7) mice. (B) Pre-B-cell colonies from *Ring1B$^{f/f}$*; *Ink4a$^{-/-}$* and *Ring1B$^{\Delta/\Delta}$*; *Ink4a$^{-/-}$* bone marrow cells. Photographs correspond to day +4 of culture and show the increased size and number of *Ink4a* mutant colonies and, in particular, of double mutant cultures. Histograms show pre-B-cell colony numbers at day +8 of culture. (C) Same experiment as in panel B but in myeloid clonogenic methylcellulose medium. Photographs were taken at day +8 of culture. Histograms depict total myeloid colony numbers in day +8 cultures.

number of *Ring1B*-deficient myeloid CFU was not affected by the lack of *Ink4a* (Fig. 5C), although the enlarged size of double mutant colonies indicated that *Ink4a* products could act by restricting the proliferative potential of maturing *Ring1B*-deficient cells. Since p19^{Arf} is not affected by Ring1B inactivation, the results confirm that the proliferative deficits of *Ring1B*-deficient hematopoietic cells are due to the upregulation of p16^{Ink4a} in maturing cells.

***Ring1B* deficiency results in an accelerated onset of hematopoietic neoplasias in the absence of *Ink4a*.** Mice with an inactive *Ink4a* locus spontaneously develop and succumb to a variety of tumors, mostly fibrosarcomas and lymphomas (62, 65). Remarkably, compound *Ring1B*; *Ink4a* mutant mice presented a quicker onset of fatal disease that lead to an acceleration of the death rate, on average 11 weeks after *Ring1B* ablation, as indicated in the survival plot shown in Fig. 6A. Four out of the six compound mutant mice which could be subjected to necropsy had developed splenomegalia and hepatomegalia (Fig. 6B, left), resulting from infiltration by cells which expressed the lymphoid marker Pax5 (Fig. 6E, right).

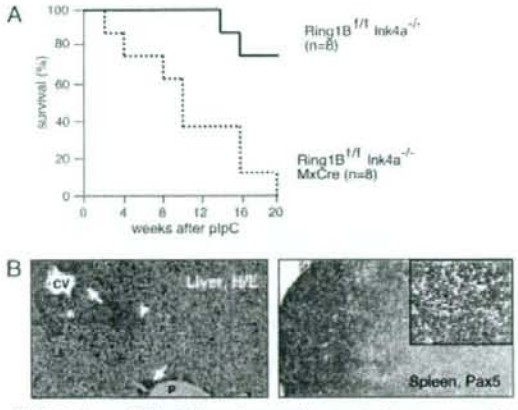

FIG. 6. Loss of Ring1B accelerates the onset of tumors associated to Ink4 inactivation. (A) Survival analysis of pIpC-injected *Ring1B*$^{f/f}$; *Ink4a*$^{-/-}$ ($n = 8$; solid lines) and *Ring1B*$^{f/f}$; *Ink4a*$^{-/-}$ *MxCre* ($n = 8$; dashed lines) mice. (B) Histochemical analysis of liver (left panel) and spleen (right panel) of a mouse in which the *Ring1B* and *Ink4a* loci are inactivated. Periportal (P) proliferation of tumor cells (arrows) with sinusoidal colonization in midzone areas (arrowhead) and marked distention of sinusoids (*) in the central vein (CV) area are shown. The normal architecture of the spleen is effaced by a diffuse proliferation of neoplastic cells. These tumor cells display positive immunostaining with Pax-5 antibody. H/E, hematoxylin and eosin stain.

The results show cooperation between the loss of function of a tumor suppressor (*Ink4a*) and the inactivation of *Ring1B*, which is in agreement with a role for *Ring1B* as a negative regulator of cell proliferation.

DISCUSSION

Elucidating the mechanisms underlying tissue self-renewal is important to understanding neoplastic processes. In this study, we provide genetic evidence supporting a distinctive role for the Polycomb protein Ring1B in the regulation of adult hematopoiesis. We find that Ring1B controls hematopoietic cell proliferation by acting as not only a positive regulator, as other PRC1 members, but also a negative regulator, depending on the maturational stage of cell differentiation. Thus, while restricting proliferation of early myeloid progenitors, Ring1B is needed for the expansion of maturing, cell lineage-committed precursors of both myeloid and lymphoid B-cell lineages. We demonstrate that these effects are mediated, at least in part, via downregulation of opposing cell cycle regulators, the G_1 cyclin D2 and its inhibitor $p16^{Ink4a}$.

Dual roles of Ring1B in positive and negative regulation of cell proliferation through downregulation of cell cycle inhibitors and activators. The hematopoietic compartment is among the tissues most affected by mutations in PcG genes, resulting in smaller thymi and spleens and a hypocellular bone marrow (36, 55). Inactivation of *Ring1B* results in a hematopoietic phenotype milder than that of other PRC1 mutant mice but equally consistent with a positive role in cell proliferation. However, the enlargement of the size of the mutant progenitor compartment indicates that Ring1B also acts as an antiproliferative regulator. The accumulation of *Ring1B*-deficient immature cells seems to be due mostly to their hyperproliferative phenotype rather than to reduced apoptosis or defective differentiation. Thus, the antiproliferative activity of Ring1B contrasts with the most prominent role of other PRC1 subunits as proliferation promoters, e.g., Bmi1. It also resembles that of the PRC2 component Eed, whose inactivation antagonizes the effects of a *Bmi1* mutation (35). Moreover, the use of an ex vivo inactivation model shows that these proliferative alterations are, at least in part, the result of *Ring1B* cell-autonomous regulated events.

In agreement with a dual role for Ring1B in negative and positive regulation of cell proliferation, we find that Ring1B targets both cell cycle activators and inhibitors. Usually, the activity of PcG proteins as promoters of cell proliferation is associated to their role as repressors of the *Ink4a* locus (23). We find that the inactivation of *Ring1B* also causes upregulation of $p16^{Ink4a}$ but not of $p19^{Arf}$, similarly to the previous observation of *Ink4a* mRNA selective derepression in constitutively *Ring1B*-deficient mouse embryos (72). In addition, our analysis demonstrates that Ring1B regulates negatively the G_1 cyclin D2 and the replication factor cdc6, two characteristic promoters of cell proliferation.

Repression by PcG complexes usually refers to the mechanisms dealing with maintenance of transcriptionally silent loci. An example is the *Ink4a/Arf* locus, which is normally inactive in proliferating cells. Association of PcG components, including Ring1B, to genomic regions of *Ink4a/Arf* and its correlation with the repressed state are considered indications of direct transcriptional control (6, 21, 31). On the other hand, negative regulation of transcriptionally active loci, such as cyclin D2 in proliferating cells, appears as a novel scenario for Polycomb repression. However, studies in *Drosophila melanogaster* show that the *Cyclin A* gene, the product of which is needed for cell cycle progression, is repressed by PRC1 subunits, Polycomb and Polyhomeotic (42). Furthermore, Polycomb was found associated to the *Cyclin A* locus, just as Ring1B and Bmi1 appear bound to regions of the *Cyclin D2* gene in ES cells and fibroblasts (5, 7). It is likely, then, that the presence of Polycomb complexes in the proximity of regulatory regions of active loci (6, 8, 50) may serve a regulatory role for fine-tuning of the transcriptional response. Regardless of the underlying mechanism(s), the finding that Ring1B negatively regulates cyclin D2 reinforces the notion that the role of PcG complexes in cell proliferation includes the regulation of components of the machinery involved in cell cycle progression.

Selective regulation of hematopoietic cell proliferation by Ring1B and other PcG products. Normal hematopoiesis displays an orchestrated use of the cell cycle machinery components in order to ensure the self-renewal and expansion activities associated with the various stages of cell differentiation of hematopoietic lineages (53). These include proliferative responses as diverse as the high self-renewal capacity and low proliferative rate of HSCs, the various proliferation rates of their progeny along their maturation, or retrieval from active proliferation of fully differentiated cells (58).

In our studies, *Ring1B* inactivation resulted in upregulation of cyclin D2 in most hematopoietic cells analyzed, except for B-cell precursors, whereas that of $p16^{Ink4a}$ was detected only in maturing B and myeloid cells but not in progenitors, thus providing an explanation for their altered proliferation rates.

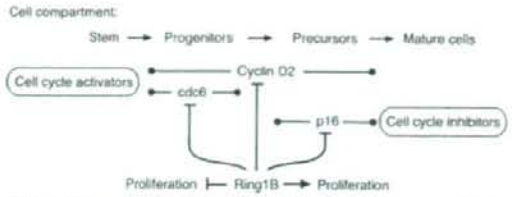

FIG. 7. Proposed model for Ring1B proliferation control during hematopoiesis. During normal hematopoiesis, Ring1B regulates progenitor and precursor cell expansion by controlling the balance between positive and negative proliferating signals. In *Ring1B*-deficient hematopoietic cells, proliferation activators cyclin D2 and cdc6 are upregulated in myeloid progenitors whereas the $p16^{Ink4a}$ proliferation inhibitor is upregulated only in more mature myeloid and lymphoid precursor cells. As a result, the early myeloid progenitor population is expanded whereas B-cell and myeloid maturing cell populations are reduced.

Mutant myeloid progenitor hyperproliferation would result from increased cyclin D2, in the absence of $p16^{Ink4a}$, as it occurs in *Cyclin D2*-transduced bone marrow cells (61). In turn, progressive accumulation of $p16^{Ink4a}$ along differentiation would abrogate the proliferative potential of the maturing progeny, despite their high content of cyclin D2, thereby resulting in a hypoplastic bone marrow. In this simple hypothesis, inhibition, but not promotion, of proliferation caused by *Ring1B* inactivation would be alleviated by loss of $p16^{Ink4a}$. Indeed, myeloid and B-cell precursors of mice bearing a coincident loss of *Ring1B* and *Ink4a* proliferate efficiently, and the reduced cellularity of *Ring1B*-deficient bone marrow is restored in the compound mutant. Instead, the hyperproliferative phenotype elicited by *Ring1B* inactivation in myeloid progenitors was not reversed by the absence of *Ink4a*. Altogether, our data support a broad regulatory role for Ring1B in the differentiation/expansion of adult hematopoietic cells by integrating signals during amplification of immature progenitors and during the expansion of their maturing progeny (Fig. 7).

The contrasting differences between hematopoietic alterations associated with Ring1B ablation and those seen in mice lacking some of their interacting partners in PRC1 complex(es), i.e., Bmi1, Mel18, M33, and Mbt1 (1, 14, 71), are likely a reflection of differential targeting in distinct cell types by complexes that vary in composition or activity. For instance, maintenance of repression of *Ink4a/Arf* in HSCs and early progenitors occurs in the absence of Ring1B but not in the absence of Bmi1 (48); another example is the p57 derepression in *Mbt1*-null myeloid progenitors (2). Given the increasing biochemical diversity of Ring1B-containing complexes (22, 47, 59), it appears that a definition of the expression pattern of their subunits throughout the differentiation stages of the various lineages will be needed for a comprehensive understanding of Polycomb complex function in hematopoiesis.

***Ring1B-Ink4a* interaction: implications for tumorigenesis.** The role of Ring1B as a proliferation promoter through repression of inhibitors of cell proliferation is consistent with the rescue of *Ring1B*-deficient bone marrow hypocellularity by *Ink4a/Arf* inactivation. This observation is reminiscent of the substantial restoration of the self-renewing capacity of HSCs (48) and of thymocytes and splenocytes of $Bmi1^{-/-}$ *Ink4a/Arf*$^{-/-}$ mice (9). Bmi1-mediated repression of *Ink4a* appears as a causal agent of primed cell proliferation in tumors, and protein expression analysis shows upregulation of Bmi1 in a variety of tumor cells. Similarly, Ring1B protein expression is increased in a variety of tumors (60), and its expression correlates with poor prognosis in a subset of malignant human cancers (24). However, the antiproliferative activity of Ring1B may also play a role in the development of neoplastic processes, as suggested by the decreased latency of tumor development in mice whose bone marrow is doubly *Ring1B* and *Ink4a/Arf* deficient compared to those lacking only *Ink4a/Arf*. Since *Ring1B* inactivation does not lead to $p19^{Arf}$ upregulation, the contribution of Ring1B in the absence of $p16^{Ink4a}$ to neoplastic events may lie in the presence of a population of progenitors with enhanced self-renewal properties susceptible of transformation (16, 32), thus cooperating with other genetic/epigenetic lesions appearing during the onset and development of tumors.

In conclusion, we have identified an antiproliferative role for Ring1B in the expansion of progenitor cells, mediated by the suppression of a positive regulator of the cell cycle machinery, which may be important in the tight control of proliferation occurring during adult hematopoiesis. It will be of interest to investigate whether this role in cell turnover takes place also in other self-renewing tissues.

ACKNOWLEDGMENTS

We thank Y. Mizutani and M. Iida for excellent technical help and T. Ikawa (RCAI) for help with quantitative PCR analysis. We thank V. Campuzano and M. Barbacid for the *RER*T^{rr} mouse line, M. Serrano for the *Ink4*$^{-/-}$ mouse line, K. Helin for anti-Bmi1 antibody, M. Sánchez-Beato for assistance with immunohistochemistry, and D. Kioussis (NIMR) for critical reading of the manuscript.

T.M. and M.R-T. were recipients of FPI and FPU fellowships, respectively, from the Ministerio de Educación y Ciencia. This work was supported by grants from the Fundación Médica Mutua Madrileña (C.C.), Plan Nacional de Investigacion Científica BFU2005-03651 (C.C.) and SAF2004-06952-CO2-01 (M.V.), the OncoCycle program from the Comunidad de Madrid (M.V.), and in part by a grant of the Genome Network Project from the Ministry of Education Culture, Sports, Science and Technology of the Japanese Government (H.K.).

REFERENCES

1. **Akasaka, T., K. Tsuji, H. Kawahira, M. Kanno, K. Harigaya, L. Hu, Y. Ebihara, T. Nakahata, O. Tetsu, M. Taniguchi, and H. Koseki.** 1997. The role of *mel-18*, a mammalian Polycomb group gene, during IL-7-dependent proliferation of lymphocyte precursors. Immunity **7**:135–146.
2. **Arai, S., and T. Miyazaki.** 2005. Impaired maturation of myeloid progenitors in mice lacking novel Polycomb group protein MBT-1. EMBO. J. **24**:1863–1873.
3. **Atsuta, T., S. Fujimura, H. Moriya, M. Vidal, T. Akasaka, and H. Koseki.** 2001. Production of monoclonal antibodies against mammalian Ring1B proteins. Hybridoma **20**:43–46.
4. **Boyer, L. A., D. Mathur, and R. Jaenisch.** 2006. Molecular control of pluripotency. Curr. Opin. Genet. Dev. **16**:455–462.
5. **Boyer, L. A., K. Plath, J. Zeitlinger, T. Brambrink, L. A. Medeiros, T. I. Lee, S. S. Levine, M. Wernig, A. Tajonar, M. K. Ray, G. W. Bell, A. P. Otte, M. Vidal, D. K. Gifford, R. A. Young, and R. Jaenisch.** 2006. Polycomb complexes repress developmental regulators in murine embryonic stem cells. Nature **441**:349–353.
6. **Bracken, A. P., D. Kleine-Kohlbrecher, N. Dietrich, D. Pasini, G. Gargiulo, C. Beekman, K. Theilgaard-Mönch, S. Minucci, B. T. Porse, J. C. Marine, K. H. Hansen, and K. Helin.** 2007. The Polycomb group proteins bind throughout the INK4A-ARF locus and are disassociated in senescent cells. Genes Dev. **21**:525–530.
7. **Bracken, A. P., N. Dietrich, D. Pasini, K. H. Hansen, and K. Helin.** 2006. Genome-wide mapping of Polycomb target genes unravels their roles in cell fate transitions. Genes Dev. **20**:1123–1136.
8. **Breiling, A., L. P. O'Neill, D. D'Eliseo, B. M. Turner, and V. Orlando.** 2004.